INSTITUTE OF PHYSICS PUBLISHING NETWORK: COMPUTATION IN NEURAL SYSTEMS

Network: Comput. Neural Syst. **12** (2001) 141–174 www.iop.org/Journals/ne PII: S0954-898X(01)22486-5

Population density methods for large-scale modelling of neuronal networks with realistic synaptic kinetics: cutting the dimension down to size

Evan Haskell[1,3], **Duane Q Nykamp**[1,4] **and Daniel Tranchina**[2,5]

[1] Courant Institute of Mathematical Sciences, New York University, New York, NY 10012, USA
[2] Department of Biology, Courant Institute of Mathematical Sciences, Center for Neural Science, New York University, New York, NY 10003, USA

E-mail: haskell@cims.nyu.edu, nykamp@math.ucla.edu and tranchina@cims.nyu.edu

Received 29 September 2000

Abstract

Population density methods provide promising time-saving alternatives to direct Monte Carlo simulations of neuronal network activity, in which one tracks the state of thousands of individual neurons and synapses. A population density method has been found to be roughly a hundred times faster than direct simulation for various test networks of integrate-and-fire model neurons with instantaneous excitatory and inhibitory post-synaptic conductances. In this method, neurons are grouped into large populations of similar neurons. For each population, one calculates the evolution of a probability density function (PDF) which describes the distribution of neurons over state space. The population firing rate is then given by the total flux of probability across the threshold voltage for firing an action potential. Extending the method beyond instantaneous synapses is necessary for obtaining accurate results, because synaptic kinetics play an important role in network dynamics. Embellishments incorporating more realistic synaptic kinetics for the underlying neuron model increase the dimension of the PDF, which was one-dimensional in the instantaneous synapse case. This increase in dimension causes a substantial increase in computation time to find the exact PDF, decreasing the computational speed advantage of the population density method over direct Monte Carlo simulation. We report here on a one-dimensional model of the PDF for neurons with arbitrary synaptic kinetics. The method is more accurate than the mean-field method in the steady state, where the mean-field approximation works best, and also under dynamic-stimulus conditions. The method is much faster than direct simulations. Limitations of the method are demonstrated, and possible improvements are discussed.

(Some figures in this article are in colour only in the electronic version; see `www.iop.org`)

[3] Current address: Cognitive Neuroscience Unit, SISSA, via Beirut 2-4, 34014 Trieste, Italy.
[4] Current address: Department of Mathematics, UCLA, Los Angeles, CA 90095, USA.
[5] To whom correspondence should be addressed.

0954-898X/01/020141+34$30.00

1. Introduction

Computational neuroscientists hope to gain an understanding of the properties of large-scale neuronal networks in part from the simulation of such networks. The time to simulate an arbitrary network by conventional methods grows quadratically with the size of the network (Hansel *et al* 1998). A substantial part of the computational load stems from the stochastic nature of signal processing in the central nervous system. For example, the input from the lateral geniculate nucleus to primary visual cortex is stochastic, and communications within the cortex are also stochastic as a consequence of unreliable synaptic transmission, random synaptic delays and random magnitudes of unitary post-synaptic conductance events. The fact that the cortex consists of a huge number of neurons, of the order of 10^8 for primary visual cortex alone, each with stochastic behaviour, suggests that a statistical mechanical approach might be of some benefit in modelling network activity. In the population density method one lumps similar neurons together into a population and then one tracks the distribution of neurons over state space instead of tracking the state of individual neurons and synapses. This distribution is described by the population density function, whose dimension depends on the underlying single-neuron model. In this method, interacting populations are coupled via their firing rates. Thus, an intrinsic limitation of the method is that it does not allow one to examine precise patterns in spike firing times, including the synchronous firing of two or more neurons.

In the population density method, the computation time depends on the number of populations rather than the number of neurons. This can result in a dramatic reduction in computation time. For example, a quarter-scale model of two hypercolumns in the cat primary visual cortex by Somers *et al* (1995) utilized a network of 2205 neurons with 180 000 synapses. The same network in a population density realization consisted of a network of 18 populations. The population density method for this orientation tuning example required about one-hundredth of the computational time of a direct Monte Carlo simulation (Nykamp and Tranchina 2000). In this model, neurons were lumped into populations on the basis of similarity of preferred orientation. In other models it might be more appropriate to lump neurons together into discrete populations according to proximity and synaptic connectivity.

In a previous paper (Nykamp and Tranchina 2000), a new population density method introduced by Knight *et al* (1996), Omurtag *et al* (2000), Sirovich *et al* (2000) and Knight (2000) for simulating large neural networks was explored. In that paper, the unitary post-synaptic conductance time course for both excitation and inhibition was assumed to be fast on the time scale of the resting membrane time constant. Thus, the unitary events were modelled by Dirac delta functions and the population density function was one-dimensional. In a later paper, Nykamp and Tranchina (2001) extended the method to handle slow inhibitory synapses by making a mean-field approximation for the slow inhibitory conductance variable. We now explore a new methodology for extending the population density method to handle realistic (arbitrary) inhibitory *and* excitatory kinetics.

Several factors motivate this extension. The excitatory conductances gated by the NMDA (*N*-methyl-*D*-aspartic acid) class of glutamate receptors have very slow kinetics (Fain 1999). NMDA receptors are found throughout the central nervous system and are thought to play an important role in synaptic plasticity. The metabotropic class of glutamate receptors gate a cation conductance through a second messenger system with slow kinetics (Fain 1999). Even so-called fast excitatory conductances gated by ionotropic receptors are not always fast on the time scale of the membrane time constant (Koch 1999). A number of studies have shown that gross qualitative features of dynamical network activity are affected dramatically by synaptic kinetics (Abbott and van Vreeswijk 1993, Treves 1993, Nykamp and Tranchina 2001, Wang 1999). Furthermore, there are theoretical reasons to believe that the details of synaptic kinetics

in general determine the stability of asynchronous activity in coupled networks of integrate-and-fire neurons (Abbott and van Vreeswijk 1993, Treves 1993).

The slow kinetics of the excitatory conductances cannot be treated by the same methods used by Nykamp and Tranchina (2001) for slow inhibitory conductances. A mean-field approximation for both the inhibitory and the excitatory conductance random variables would remove all intrinsic noise from the system. The only remaining randomness would be from the initial random distribution of neurons over voltage. As a consequence, the firing rate would depend on the initial probability density function (PDF). Moreover, the leakage term would tend to synchronize the population (Knight 1972). One could avoid these problems by injecting artificial extrinsic noise into the system (e.g., Abbott and van Vreeswijk (1993)). The method described in this paper is an alternative method that keeps the details of the intrinsic synaptic noise in the system.

Allowing for realistic synaptic kinetics in the population density method leads to a high-dimensional partial differential-integral equation for the evolution of the PDF. Increasing the dimension of the system leads to an exponential increase in computational time. We present here a one-dimensional model for the high-dimensional stochastic process given by neurons with non-instantaneous synaptic kinetics. The evolution equation for the corresponding one-dimensional PDF is a partial differential-integral equation. We show how this equation can be approximated by an advection–diffusion–dispersion equation. We demonstrate the accuracy, computational efficiency and limitations of our one-dimensional model.

2. The integrate-and-fire neuron

As in previous models (Nykamp and Tranchina 2000, Knight *et al* 1996, Omurtag *et al* 2000, Sirovich *et al* 2000, Knight 2000, Brunel and Hakim 1999), the implementation of the population density approach is based on an integrate-and-fire, single-compartment (point) neuron. We model the synaptic input as a current injection. The essence of the dimension problem is captured with this simplification. Further work will be required to incorporate slow synaptic conductances in the population density framework.

The temporal evolution of a neuron's transmembrane voltage, $V(t)$, is given by the stochastic differential equation (SDE) (for SDEs throughout this paper, upper case letters are used to indicate random quantities):

$$c\frac{\mathrm{d}V}{\mathrm{d}t} = -g_{\mathrm{r}}(V - \mathcal{E}_{\mathrm{r}}) + E(t) - I(t), \tag{1}$$

where c is the membrane capacitance, g_{r} and $\mathcal{E}_{\mathrm{r}}$ are the resting membrane conductance and equilibrium potential, and $E(t)$ and $I(t)$ are the stochastic excitatory and inhibitory synaptic currents, respectively. When $V(t)$ reaches a fixed threshold voltage v_{th}, the neuron is said to fire a spike, and the voltage is reset to the voltage v_{reset}. Since we model the inhibitory synaptic input as current injection rather than conductance modulation, we impose a lower bound $\mathcal{E}_{\mathrm{i}}$ on the membrane potential.

2.1. Synaptic currents

The synaptic currents, $E(t)$ and $I(t)$, vary in response to excitatory and inhibitory input, respectively. Upon the arrival of a synaptic input, the synaptic current increases in magnitude and then decays exponentially. This rise of the current can be modelled as either an instantaneous jump (which we call first-order kinetics) or a smooth exponential increase (second-order kinetics). The theory developed in this paper does not depend on the waveforms

for the unitary post-synaptic current events. We denote the rise and decay time constants by τ_r and τ_d respectively ($\tau_r < \tau_d$).

For first-order kinetics, the evolution of the excitatory synaptic current, $E(t)$, is governed by

$$\tau_d^e \frac{dE}{dt} = -E(t) + \sum_{k=1}^{N_e} Q_e^k \delta(t - T_e^k), \tag{2}$$

and similarly for the inhibitory synaptic current, $I(t)$:

$$\tau_d^i \frac{dI}{dt} = -I(t) + \sum_{k=1}^{N_i} Q_i^k \delta(t - T_i^k), \tag{3}$$

where $N_{e/i}$ is the total number of excitatory/inhibitory unitary synaptic events; $T_{e/i}^k$ is the random arrival time of the kth excitatory/inhibitory unitary synaptic event and $Q_{e/i}^k$ denotes the total charge delivered to the synapse by an unitary excitatory/inhibitory event. Instantaneous synaptic kinetics correspond to the case in which $\tau_d^{e/i} = 0$. In this case the synaptic events are modelled by Dirac delta functions:

$$E(t) = \sum_{k=1}^{N_e} Q_e^k \delta(t - T_e^k), \qquad I(t) = \sum_{k=1}^{N_i} Q_i^k \delta(t - T_i^k). \tag{4}$$

For second-order kinetics, we introduce the auxiliary variable $S(t)$. The evolution of the excitatory synaptic current, $E(t)$, is governed by

$$\tau_d^e \frac{dE}{dt} = -E(t) + S(t) \tag{5}$$

$$\tau_r^e \frac{dS}{dt} = -S(t) + \sum_{k=1}^{N_e} Q_e^k \delta(t - T_e^k), \tag{6}$$

and similarly for the inhibitory synaptic current $I(t)$.

These ODEs for the synaptic currents imply that

$$E(t) = \sum_{k=1}^{N_e} Q_e^k h_e(t - T_e^k), \qquad I(t) = \sum_{k=1}^{N_i} Q_i^k h_i(t - T_i^k) \tag{7}$$

where the waveform $h_{e/i}(t)$ is given by either a single exponential (8) for first-order kinetics or a difference of exponentials (9) for second-order kinetics:

$$h(t) = \frac{1}{\tau_d} e^{-\frac{t}{\tau_d}} H(t) \tag{8}$$

or

$$h(t) = \frac{1}{\tau_d - \tau_r} \left(e^{-\frac{t}{\tau_d}} - e^{-\frac{t}{\tau_r}} \right) H(t), \tag{9}$$

where $H(t)$ is the Heaviside step function. Note that, by construction, $h_{e/i}(t)$ has unit area. To take into account the random fluctuations in unitary excitatory post-synaptic current (EPSC) events and unitary inhibitory post-synaptic current events, the $Q_{e/i}^k$ (total charge delivered per event) are independent identically distributed random variables (IIDRVs). The arrival time of the post-synaptic current events, $T_{e/i}^k$, are random variables governed by an inhomogeneous Poisson process. The Poisson assumption is valid in the regime where each neuron receives random input from numerous presynaptic neurons with conditionally independent spike trains.

To facilitate the presentation, we combine (1) and (7), rewriting the resulting SDE as

$$\frac{\mathrm{d}V}{\mathrm{d}t} = \left\{ -\frac{1}{\tau_m}(V - \mathcal{E}_\mathrm{r}) + \sum_{k=1}^{N_\mathrm{e}} A_\mathrm{e}^k h_\mathrm{e}(t - T_\mathrm{e}^k) - \sum_{k=1}^{N_\mathrm{i}} A_\mathrm{i}^k h_\mathrm{e}(t - T_\mathrm{i}^k) \right\} \qquad \text{for} \quad \mathcal{E}_\mathrm{i} < v < v_\mathrm{th}, \tag{10}$$

where $A_{\mathrm{e/i}} = Q_{\mathrm{e/i}}/c$, and $\tau_m = g_\mathrm{r}/c$ is the resting membrane time constant. Since the $A_{\mathrm{e/i}}^k$ are random variables, we define the density function for $A_{\mathrm{e/i}}$, $f_{A_{\mathrm{e/i}}}(x)$. Details of this distribution are given in appendix A.

2.2. Mean-field and Monte Carlo methods

In this paper, we compare population density results with direct Monte Carlo simulations and also with a mean-field approximation for the activity of populations of neurons. The mean-field method assumes that there are many synaptic events on the time scale of the synaptic time constant, so that the post-synaptic current is well approximated by its mean. In a mean-field approximation for activity in a network of interacting populations of integrate-and-fire neurons corresponding to the population density network, the mean excitatory and inhibitory synaptic currents in each population are expressed as functionals of the firing rates of the presynaptic populations (Bressloff and Coombes 2000). In the case of a single exponential unitary event, the evolution equation for the mean excitatory current, $\mu_\mathrm{E}(t)$, is obtained by taking the expected value of (2) over the random charges, Q_e^k, and over the random arrival times, T_e^k, which are governed by a modulated (inhomogeneous) Poisson process. The result is

$$\tau_\mathrm{d}^\mathrm{e} \frac{\mathrm{d}\mu_\mathrm{E}}{\mathrm{d}t} = -\mu_\mathrm{E}(t) + \mu_{Q_\mathrm{e}} \nu_\mathrm{e}(t) \tag{11}$$

where μ_{Q_e} is the average total charge injected by a unitary event, and $\nu_\mathrm{e}(t)$ is the sum of the rates of synaptic inputs from all the presynaptic populations. The evolution for $\mu_I(t)$ is similar.

The firing rate for any population, $r(t)$, is computed by making the approximation that the net synaptic currents change slowly on the time scale of the interspike interval. Thus, $r(t)$ is computed by (i) holding the net synaptic currents fixed at their expected values at time t; (ii) calculating the time T to cross spike threshold starting from the reset voltage, including any refractory period τ_ref and (iii) setting the firing rate $r(t)$ equal to $1/T$. The resulting nonlinear equation that gives firing rate, r, as a function of synaptic currents is

$$r(t) = \frac{1}{\tau_m \ln\left[\frac{V_\mathrm{reset} - \mathcal{E}_\mathrm{r} - (\mu_\mathrm{E}(t) - \mu_I(t))/g_\mathrm{r}}{V_\mathrm{th} - V_\mathrm{reset} - (\mu_\mathrm{E}(t) - \mu_I(t))/g_\mathrm{r}}\right] + \tau_\mathrm{ref}}, \tag{12}$$

for $[(\mu_\mathrm{E}(t) - \mu_I(t))/g_\mathrm{r}] > (V_\mathrm{th} - V_\mathrm{reset})$, and $r(t) = 0$ otherwise.

In our Monte Carlo simulations, the external input to a population consists of a Poisson train of events with random magnitudes. When populations are coupled together, precise spike times are determined and a random delay and magnitude are chosen for each post-synaptic event. The same distribution functions are used for delays and magnitudes in the PDF and Monte Carlo methods.

3. The population density model

With non-instantaneous synaptic kinetics, the state of a neuron is described not only by its membrane potential $V(t)$, but also by one (first-order kinetics) or two (second-order kinetics) variables for the state of each of the synaptic currents $E(t)$ and $I(t)$. Thus, the state space for the neuron is high-dimensional. We point out that in the population density framework,

the population firing rate is given by the total flux of probability across the threshold voltage, v_{th}. This flux depends on the marginal density of the membrane potential $V(t)$, $\rho_V(v,t)$. We develop a one-dimensional model below which gives an approximate evolution equation for $\rho_V(v,t)$.

As in Nykamp and Tranchina (2000), we assume that the populations consist of a large number of biophysically identical neurons. We also assume that the populations are sparsely connected. That is, any pair of neurons in a given population have very few presynaptic neurons in common. The assumption of sparse connectivity is required by the assumption of conditional independence of the input events across all neurons (Nykamp and Tranchina 2000). It has been demonstrated that, in practice, the connectivity of model networks need not be terribly sparse in order to get accurate population density results (Nykamp and Tranchina 2000).

We begin by stating in section 3.1 the full high-dimensional evolution equation. Rather than embarking on the computationally intensive effort of numerically solving this evolution equation, we develop a one-dimensional model for $\rho_V(v,t)$ in section 3.2. An exact evolution equation for $\rho_V(v,t)$ in a related simpler problem will serve as a basis for our one-dimensional model.

3.1. The high-dimensional evolution equation

Before developing our one-dimensional model, we state the exact high-dimensional evolution equation. For simplicity, let us consider the case of first-order synaptic input for both excitation and inhibition. In this case, the state of a neuron is determined by its membrane potential $V(t)$, a single-state variable for the excitatory current $E(t)$, and a single-state variable for the inhibitory current $I(t)$. For convenience of presentation, we replace the state variables $E(t)$ and $I(t)$ with $X(t) = E(t)/c$ and $Y(t) = I(t)/c$ (units of V s^{-1}), respectively.

This three-dimensional state space gives rise to a three-dimensional PDF for the state of a neuron, $\rho(v,x,y,t)$, where

$$\rho(v,x,y,t)\,\mathrm{d}v\,\mathrm{d}x\,\mathrm{d}y = \Pr\{V(t) \in (v, v+\mathrm{d}v), X(t) \in (x, x+\mathrm{d}x), Y(t) \in (y, y+\mathrm{d}y)\} \tag{13}$$

for $v \in (\mathcal{E}_{\text{i}}, v_{\text{th}})$, $x \in (0,\infty)$ and $y \in (0,\infty)$. The corresponding evolution equation for this PDF is the following three-dimensional conservation equation:

$$\frac{\partial \rho}{\partial t}(v,x,y,t) = -\nabla \cdot \vec{J}(v,x,y,t) + \delta(v - v_{\text{reset}})J_U(\tau_{\text{ref}},x,y,t) \tag{14}$$

where $\vec{J}(v,x,y,t) = (J_V(v,x,y,t), J_X(v,x,y,t), J_Y(v,x,y,t))$ is the flux of probability per unit area at the point (v,x,y) in the three-dimensional state space, and $J_U(\tau_{\text{ref}},x,y,t)$ is the flux of neurons returning from a refractory period. The components of the flux vector $\vec{J}(v,x,y,t)$ represent the flux across voltage, flux across normalized excitatory synaptic current, and flux across normalized inhibitory synaptic current respectively:

$$J_V(v,x,y,t) = -\frac{1}{\tau_m}(v-\mathcal{E}_{\text{r}})\rho(v,x,y,t) + x\rho(v,x,y,t) - y\rho(v,x,y,t) \tag{15}$$

$$J_X(v,x,y,t) = -\frac{1}{\tau_{\text{d}}^{\text{e}}}x\rho(v,x,y,t) + \nu_{\text{e}}(t)\int_0^x \tilde{F}_{A_{\text{e}}}((x-x')\tau_{\text{d}}^{\text{e}})\rho(v,x',y,t)\,\mathrm{d}x' \tag{16}$$

$$J_Y(v,x,y,t) = -\frac{1}{\tau_{\text{d}}^{\text{i}}}y\rho(v,x,y,t) + \nu_{\text{i}}(t)\int_0^y \tilde{F}_{A_{\text{i}}}((y-y')\tau_{\text{d}}^{\text{i}})\rho(v,x,y',t)\,\mathrm{d}y' \tag{17}$$

where $\tilde{F}_{A_{\text{e/i}}}(x) = \int_x^\infty f_{A_{\text{e/i}}}(a)\,\mathrm{d}a$ is the complementary cumulative distribution function for $A_{\text{e/i}}$.

A neuron fires a spike when its voltage crosses v_{th}, so the total flux across threshold is the population firing rate:

$$r(t) = \iint J_V(v_{\text{th}}, x, y, t)\,\mathrm{d}x\,\mathrm{d}y. \tag{18}$$

Replacing $J_V(v_{\text{th}}, x, y, t)$ in (18) with the expression given in equation (15) shows that the firing rate depends on the marginal flux of probability across the threshold potential v_{th}:

$$r(t) = \left[-\frac{1}{\tau_m}(v_{\text{th}} - \mathcal{E}_{\text{r}}) + \mu_{X|V}(v_{\text{th}}, t) - \mu_{Y|V}(v_{\text{th}}, t)\right]\rho_V(v_{\text{th}}, t), \tag{19}$$

where $\mu_{X|V}(v, t)$ and $\mu_{Y|V}(v, t)$ are the means of the state variables $X(t)$ and $Y(t)$, respectively, given the membrane potential $V(t)$. That is to say, the firing rate can be found by considering the flux of probability across threshold of the marginal probability density for the membrane potential $V(t)$: $r(t) = J_V(v_{\text{th}}, t)$. In a full treatment of the problem, the firing rate cannot be found from $\rho_V(v_{\text{th}}, t)$ alone as it also depends on two unknown functions $\mu_{X|V}(v_{\text{th}}, t)$ and $\mu_{Y|V}(v_{\text{th}}, t)$.

This three-dimensional system would become five-dimensional if a more realistic difference of exponentials waveform (second-order kinetics) were used for the unitary post-synaptic events. Including additional currents, such as a NMDA excitatory current in addition to an AMPA (alpha-amino-3-hydroxy-5-methyl-4 isoxazole proprionic acid) excitatory current, would further increase the dimension. Rather than solve such computationally intensive high-dimensional systems, we focus on the one-dimensional voltage marginal density function $\rho_V(v, t)$. This one-dimensional model is not obtained by starting with (14), but rather by considering a different but related stochastic process.

3.2. Evolution equation for the one-dimensional model

The evolution equation for the one-dimensional model corresponding to (14) is

$$\frac{\partial \rho_V}{\partial t}(v, t) = -\frac{\partial}{\partial v}J(v, t) + \delta(v - v_{\text{reset}})J_U(\tau_{\text{ref}}, t), \tag{20}$$

with corresponding firing rate $r(t) = J_V(v_{\text{th}}, t)$. The flux of neurons returning from a refractory state is given by the firing rate $J_U(\tau_{\text{ref}}, t) = r(t - \tau_{\text{ref}})$.

In order to develop this one-dimensional model, we begin in section 3.2.1 by considering the simpler problem obtained by eliminating the lower bound on voltage and by removing the voltage reset. We then in section 3.2.4 include a voltage threshold, voltage reset and a limit on the level of membrane hyperpolarization. The corresponding evolution equation for the instantaneous synapse problem can be found by using the techniques in Nykamp and Tranchina (2000) and Brunel and Hakim (1999).

3.2.1. Without voltage reset or lower boundary. When voltage threshold and reset in (10) are removed, $V(t)$ moves randomly on the real line. In this case, the voltage $V(t)$ can be thought of as Poisson shot noise arising from numerous independent events. We will demonstrate that, as a consequence, the characteristic function of the random voltage has a surprisingly tractable analytical form. This characteristic function can be differentiated with respect to time and then inverse-Fourier-transformed to give an evolution equation for the voltage density function of integrate-and-fire neurons.

The evolution equation for $\rho_V(v, t)$ in this unconstrained random motion problem will serve as a basis for a one-dimensional model for the actual problem of interest.

The evolution equation for the one-dimensional model corresponding to (20) when there is no voltage threshold is

$$\frac{\partial \rho_v}{\partial t}(v,t) = -\frac{\partial}{\partial v} J(v,t). \tag{21}$$

For the sake of simplifying notation in this presentation, we will develop the evolution equation for excitatory input only. The addition of the inhibitory input is similar. To emphasize this similarity, we remove the subscripts for excitation. We find the evolution equation for $\rho_v(v,t)$ by considering its corresponding characteristic function, $\hat{\rho}_v(\xi,t)$:

$$\hat{\rho}_v(\xi,t) = \int \rho_v(v,t) \mathrm{e}^{-\mathrm{i}\xi v}\, \mathrm{d}v \tag{22}$$

$$= \mathbb{E}\left[\mathrm{e}^{-\mathrm{i}\xi V(t)}\right]. \tag{23}$$

We note that the expression for the characteristic function is the expected value of $\mathrm{e}^{-\mathrm{i}\xi V(t)}$, a function of our random variable $V(t)$. We solve (10) explicitly to find

$$V(t) = \mathcal{E}_\mathrm{r} + \sum_{k=1}^{N} A_k q(t - T_k), \tag{24}$$

where $q(t) = h(t) * \left(\mathrm{e}^{-\frac{t}{\tau_m}} H(t)\right)$, and $*$ denotes the convolution operator. We emphasize that there are three classes of random variables in the expression for $V(t)$: the random number of events, N, the arrival times of those events, T_k, and the random amplitudes of those events, A_k. Because the arrival times are governed by a Poisson process, the number of events N is Poisson distributed. We insert (24) for $V(t)$ into (23) to obtain and expected value expression in which the random variables are represented explicitly:

$$\hat{\rho}_v(\xi,t) = \mathbb{E}\left[\exp\left\{-\mathrm{i}\xi\left(\mathcal{E}_\mathrm{r} + \sum_{k=1}^{N} A_k q(t-T_k)\right)\right\}\right]. \tag{25}$$

If we first condition on N, that is fix the number of events, then $\{T_1, T_2, \ldots, T_N\}$ are IIDRVs, as are $\{A_1, A_2, \ldots, A_N\}$. With this conditioning in place, we are taking the expected value of a product of IIDRVs. For any set of IIDRVs, $\{Z_1, Z_2, \ldots, Z_M\}$, we note that $\mathbb{E}\left[\prod_{k=1}^{M} Z_k\right] = (\mathbb{E}[Z])^M$, where Z denotes any arbitrary Z_k. The conditioning on N requires that we first take the expected value over random variables A and T and then over N:

$$\hat{\rho}_v(\xi,t) = \exp(-\mathrm{i}\xi\mathcal{E}_\mathrm{r})\,\mathbb{E}\left(\mathbb{E}\left[\exp\left\{-\mathrm{i}\xi\sum_{k=1}^{N} A_k q(t-T_k)\right\}\middle| N=n\right]\right) \tag{26}$$

$$= \exp(-\mathrm{i}\xi\mathcal{E}_\mathrm{r})\,\mathbb{E}\left\{\left(\mathbb{E}\left[\mathrm{e}^{-\mathrm{i}\xi A q(t-T)}\right]\right)^N\right\}. \tag{27}$$

To take the expected value in (27) over T, we use the fact that the density function $f_T(t)$ for the random arrival times is given by the rate of events (probability per unit time) at time t divided by the integral of the rate up to time t. Thus,

$$f_T(t') = \nu(t')/\mu(t) \qquad \text{for} \quad -\infty < t' < t, \tag{28}$$

where $\mu(t) = \int_{-\infty}^{t} \nu(t')\,\mathrm{d}t'$. We point out that the expected value for random number of events N up to time t is given by $\mu(t)$. The expected value in (27) over random event amplitude A is performed using the previously defined density function $f_A(x)$. Thus, the overall inner expected value in (27), still keeping N fixed, is given by

$$\mathbb{E}\left[\mathrm{e}^{-\mathrm{i}\xi A q(t-T)}\right] = \int_0^\infty \mathrm{d}x\, f_A(x) \int_{-\infty}^{t} \mathrm{e}^{-\mathrm{i}\xi x q(t-t')} \frac{\nu(t')}{\mu(t)}\,\mathrm{d}t'. \tag{29}$$

Substituting (29) into (27) gives

$$\hat{\rho}_V(\xi,t) = \exp(-\mathrm{i}\xi\mathcal{E}_\mathrm{r})\,\mathbb{E}\left[\left(\int_0^\infty \mathrm{d}x\; f_A(x)\int_{-\infty}^t \mathrm{e}^{-\mathrm{i}\xi x q(t-t')}\frac{\nu(t')}{\mu(t)}\,\mathrm{d}t'\right)^N\right]. \tag{30}$$

The expectation computation in (30) is of the form $\mathbb{E}\left[z^N\right]$, where

$$z = \int_0^\infty \mathrm{d}x\; f_A(x)\int_{-\infty}^t \mathrm{e}^{-\mathrm{i}\xi x q(t-t')}\frac{\nu(t')}{\mu(t)}\,\mathrm{d}t'. \tag{31}$$

To proceed, since N is Poisson distributed with mean $\mu(t)$, it follows that

$$\mathbb{E}[z^N] = \sum \frac{1}{k!}(z\mu(t))^k\,\mathrm{e}^{-\mu(t)} \tag{32}$$

$$= \mathrm{e}^{z\mu(t)}\mathrm{e}^{-\mu(t)} \tag{33}$$

$$= \exp\left[z\mu(t) - \mu(t)\right]. \tag{34}$$

Using result (34) in (30) gives

$$\hat{\rho}_V(\xi,t) = \exp(-\mathrm{i}\xi\mathcal{E}_\mathrm{r})\exp\left\{\int_0^\infty \mathrm{d}x\; f_A(x)\int_{-\infty}^t \mathrm{d}t'\nu(t')\mathrm{e}^{-\mathrm{i}\xi x q(t-t')} - \mu(t)\right\} \tag{35}$$

$$= \exp(-\mathrm{i}\xi\mathcal{E}_\mathrm{r})\exp\left\{\int_0^\infty \mathrm{d}x\; f_A(x)\int_{-\infty}^t \mathrm{d}t'\nu(t')\left[\mathrm{e}^{-\mathrm{i}\xi x q(t-t')} - 1\right]\right\}. \tag{36}$$

In going from (35) to (36) we used the definition of $\mu(t)$ and the fact that $\int_0^\infty f_A(x) = 1$.

Equation (36) is the characteristic function for the voltage marginal PDF. To find the evolution equation for the voltage marginal PDF, we differentiate this characteristic function with respect to time and take the inverse Fourier transform. We note that $q(t)$ as given above satisfies the differential equation $\frac{\mathrm{d}q}{\mathrm{d}t} = -\frac{1}{\tau_m}q(t) + h(t)$, since $q(t)$ is the unitary post-synaptic potential waveform (i.e. the solution to (10) for one event when $\mathcal{E}_\mathrm{r} = 0$ mV and $A = 1$ mV). Using this fact, the temporal derivative (here, it is assumed that $h(t)$ is not a Dirac delta function and hence $q(0) = 0$) is

$$\frac{\partial\hat{\rho}_V}{\partial t} = \hat{\rho}_V(\xi,t)\int_0^\infty \mathrm{d}x\; f_A(x)\int_{-\infty}^t \mathrm{d}t'\nu(t')\mathrm{e}^{-\mathrm{i}\xi x q(t-t')}\left[-\mathrm{i}\xi x\frac{\mathrm{d}}{\mathrm{d}t}q(t-t')\right] \tag{37}$$

$$= \hat{\rho}_V(\xi,t)\int_0^\infty \mathrm{d}x\; f_A(x)\int_{-\infty}^t \mathrm{d}t'\nu(t')\mathrm{e}^{-\mathrm{i}\xi x q(t-t')}(-\mathrm{i}\xi)x \times\left[-\frac{1}{\tau_m}q(t-t') + h(t-t')\right] \tag{38}$$

$$= \frac{\mathrm{i}\xi}{\tau_m}\int_0^\infty x f_A(x)\,\mathrm{d}x\int_{-\infty}^t \nu(t')q(t-t')\mathrm{e}^{-\mathrm{i}\xi x q(t-t')}\,\mathrm{d}t'\hat{\rho}_V(\xi,t) - \mathrm{i}\xi\int_0^\infty x f_A(x)\,\mathrm{d}x\int_{-\infty}^t \nu(t')h(t-t')\mathrm{e}^{-\mathrm{i}\xi x q(t-t')}\,\mathrm{d}t'\hat{\rho}_V(\xi,t) \tag{39}$$

$$= -\frac{\xi}{\tau_m}\frac{\partial\hat{\rho}_V}{\partial\xi} - \frac{\mathrm{i}\xi}{\tau_m}\mathcal{E}_\mathrm{r}\hat{\rho}_V - \mathrm{i}\xi\int_0^\infty x f_A(x)\,\mathrm{d}x \times\int_{-\infty}^t \nu(t')h(t-t')\mathrm{e}^{-\mathrm{i}\xi x q(t-t')}\,\mathrm{d}t'\hat{\rho}_V(\xi,t). \tag{40}$$

In the transition between equations (39) and (40) we used the fact that the ξ derivative of the characteristic function (36) is

$$\frac{\partial\hat{\rho}_V}{\partial\xi} = -\mathrm{i}\mathcal{E}_\mathrm{r}\hat{\rho}_V(\xi,t) - \mathrm{i}x\int_0^\infty \mathrm{d}x\; f_A(x)\int_{-\infty}^t \mathrm{d}t'\nu(t')q(t-t')\mathrm{e}^{-\mathrm{i}\xi x q(t-t')}\hat{\rho}_V(\xi,t). \tag{41}$$

Now that we have an evolution equation (40) for the characteristic function (36), we need only take the inverse Fourier transform of (40) to find the evolution equation for the voltage marginal PDF. This evolution equation specialized for excitatory input is

$$\frac{\partial \rho_V}{\partial t} = -\frac{\partial}{\partial v}\left\{-\frac{1}{\tau_m}(v - \mathcal{E}_r)\rho_V(v,t) + J_e(v,t)\right\}, \tag{42}$$

where

$$J_e(v,t) = \int_{-\infty}^{t} \mathrm{d}t' h_e(t-t')\nu_e(t') \int_0^{\infty} \mathrm{d}x\, x f_{A_e}(x)\, \rho_V(v - x q_e(t-t'), t). \tag{43}$$

Substituting the expression for the flux (43) into the model evolution equation (42) leads to a partial differential integral equation for the evolution of $\rho_V(v,t)$. In the special case where the unitary post-synaptic current event amplitude is fixed rather than random, the excitatory flux is of a particularly simple form:

$$J_e(v,t) = \int_{-\infty}^{t} \mathrm{d}t'\, \nu_e(t')\, A_e h_e(t-t')\, \rho_V(v - A_e q_e(t-t'), t). \tag{44}$$

Equation (44) for the excitatory component of the probability flux indicates that the present flux includes attenuated surviving effects from the history of earlier unitary post-synaptic current events. Note that, in (44), $A_e h_e(t-t')$ is the surviving post-synaptic current at time t from a unitary event at time t', and $A_e q_e(t-t')$ is the surviving post-synaptic potential response to that event. An alternative approach towards the density function for shot noise can be found in Grzywacz *et al* (1988).

3.2.2. Partial differential equation approximation for the evolution equation. In an effort to circumvent the computational demands required to numerically solve such an equation, we expand $\rho_V(v,t)$ in a Taylor series around v and rewrite the expression for the excitatory flux (43) as

$$J_e(v,t) = \sum_{j=0}^{\infty}\left[\frac{(-1)^j}{j!}\mu_{A_e^{j+1}} \int_{-\infty}^{t} h_e(t-t') q_e^j(t-t')\nu_e(t')\,\mathrm{d}t'\right]\frac{\partial^j \rho_V}{\partial v^j}. \tag{45}$$

If inhibitory synaptic input is added as well, each excitatory term in (42) will have a corresponding inhibitory term like those in (45) added to it.

The first three terms of the sum in (45) correspond to the excitatory advection (drift), diffusion and dispersion, respectively. As demonstrated below, an excellent approximation for unitary post-synaptic currents of physiological magnitude is obtained by keeping only these first three terms provided that the EPSP size is not too large. The coefficients of the jth partial derivative of $\rho_V(v,t)$ with respect to v decay rapidly for physiologically reasonable EPSP magnitudes as j increases; hence, the higher-order terms in the Taylor series expansion are small. When ν_e is constant, the coefficients of $\frac{\partial^j \rho_V}{\partial v^j}$ can be evaluated easily. For example, when the average unitary EPSP size is 0.5 mV and the unitary post-synaptic current is a single exponential with a decay time constant equal to $\tau_m/2$, the first five normalized coefficients in (45) are 1.0000, −0.4167, 0.1250, −0.0313 and 0.0069. Notice that the magnitude of the fourth term is only 3% of the advection (first-term) coefficient. Figure 1 shows the normalized magnitude of the first few coefficients as a function of the EPSP size and synaptic time constant of decay. By truncating the Taylor series after three terms, we are able to gain an accurate approximation to (45) that is numerically more advantageous to compute than (43). (In our numerical method we do not incur any additional computational cost by keeping the dispersion term. Our numerical method employs an upwind difference scheme for the derivative of the

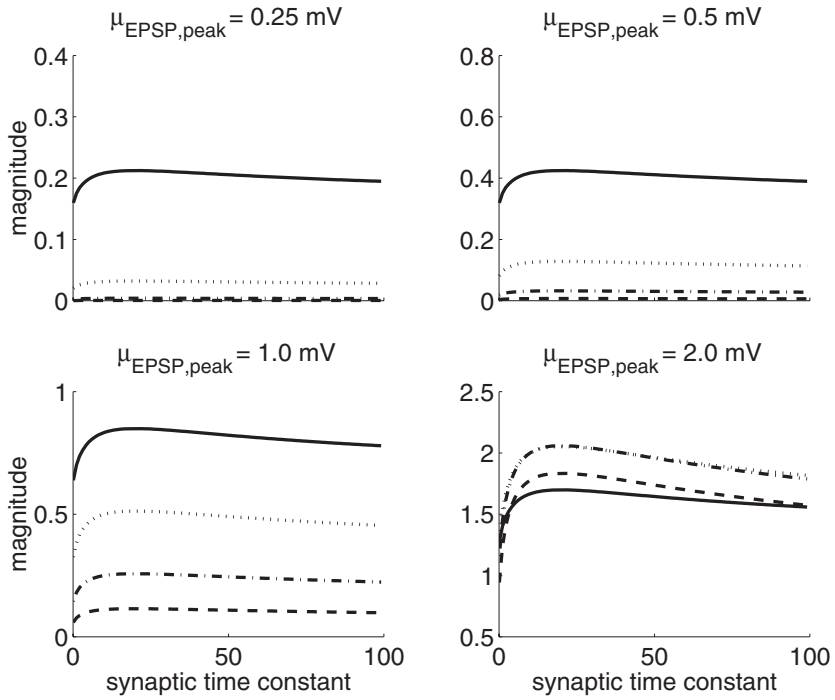

Figure 1. The first few steady-state coefficients from the Taylor series for the excitatory flux normalized by the first coefficient as a function of the time constant of synaptic decay. Above each panel the mean peak response size is given. As the peak response increases, the higher-order terms become more relevant. The curves represent the second term (solid curve), third term (dotted curve), fourth term (dashed-dotted curve), and fifth term (dashed curve).

advection flux in order to ensure stability in the absence of synaptic input. This gives a pentadiagonal matrix equation to be solved at each time step. With the dispersion term, the matrix is still pentadiagonal.)

We may rewrite the advection–diffusion–dispersion approximation for the excitatory flux in (45) as

$$J_{\mathrm{e}}(v,t) \approx c_1^{\mathrm{e}} a_{\mathrm{e}}(t)\rho(v,t) + 2c_2^{\mathrm{e}} D_{\mathrm{e}}(t)\frac{\partial \rho}{\partial v}(v,t) + 3c_3^{\mathrm{e}} F_{\mathrm{e}}(t)\frac{\partial^2 \rho}{\partial v^2}(v,t) \tag{46}$$

where $c_1^{\mathrm{e}} a_{\mathrm{e}}(t),\ 2c_2^{\mathrm{e}} D_{\mathrm{e}}(t),\ 3c_3^{\mathrm{e}} F_{\mathrm{e}}(t)$ are the coefficients corresponding to advection, diffusion and dispersion, respectively:

$$a_{\mathrm{e}}(t) = \int_{-\infty}^{t} h_e(t-t')\nu_e(t')\,\mathrm{d}t' \tag{47}$$

$$D_{\mathrm{e}}(t) = \int_{-\infty}^{t} q_e(t-t')h_e(t-t')\nu_e(t')\,\mathrm{d}t' \tag{48}$$

$$F_{\mathrm{e}}(t) = \int_{-\infty}^{t} q_e^2(t-t')h_e(t-t')\nu_e(t')\,\mathrm{d}t' \tag{49}$$

$$c_k^{\mathrm{e}} = (-1)^{k-1}\frac{1}{k!}\mu_{A_{\mathrm{e}}^k}. \tag{50}$$

In appendix E, we discuss the relationship between the coefficients above and the moments of the distribution function for $V(t)$ as determined by the SDE (1).

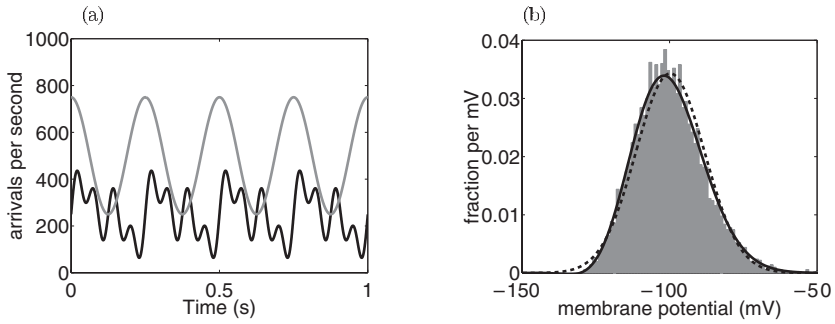

Figure 2. A snapshot of the population density function compared with the histogram formed by one Monte Carlo simulation of 5000 'neurons'. In (*b*) the advection–diffusion–dispersion (solid curve) and diffusion (dashed curve) approximations are shown. The bin width for the histogram in (*b*) is 1 mV. The arrival rate of excitation (dark curve) and inhibition (grey curve) are shown in (*a*). Parameters: $\tau_e = 5$ ms, $\tau_i = 10$ ms, $\mu_{EPSP,peak} = 4$ mV, $\mu_{IPSP,peak} = 1$ mV. This snapshot was taken at $t = 150$ ms.

In the case of instantaneous synaptic kinetics, the advection–diffusion–dispersion approximation to the corresponding one-dimensional process is

$$J_e(v,t) \approx \nu_e(t)\, c_1^e \rho(v,t) + \nu_e(t)\, c_2^e \frac{\partial \rho}{\partial v}(v,t) + \nu_e(t)\, c_3^e \frac{\partial^2 \rho}{\partial v^2}(v,t), \tag{51}$$

where c_k^e are as above. The inhibitory flux expression is similar. We show in appendix D that, in the limit of instantaneous synaptic kinetics, our one-dimensional model converges to the flux expression for the case of instantaneous synaptic kinetics.

3.2.3. Accuracy of the advection–diffusion–dispersion approximation. To demonstrate the accuracy of the advection–diffusion–dispersion approximation, we show in figure 2(*a*) a snapshot comparing different estimates of the PDF for a non-instantaneous synapse problem without voltage reset and without a lower boundary for V. In this example, the arrival times of excitatory and inhibitory events are governed by independent modulated Poisson processes at prescribed rates. Figure 2(*a*) shows the synaptic input rates. (In general, the prescribed input rates in our illustrations are arbitrary, and they were chosen as a convenient way of providing temporally rich input.) One estimate of the PDF in 2(*b*) (histogram) is a relative frequency estimate obtained by a Monte Carlo simulation with 5000 uncoupled neurons. The other (solid curve) is obtained from solving (21) with the advection–diffusion–dispersion approximation (46). We see near-perfect agreement between our numerical solution of the advection–diffusion–dispersion evolution equation and Monte Carlo simulation.

In this example, we chose a large size for the unitary excitatory event ($\mu_{EPSP,peak} = 4$ mV) in order to show that our advection–diffusion–dispersion approximation does well even under these circumstances. This is a surprising result in light of the data presented in figure 1. For large enough EPSP (around 2 mV), skew becomes evident in the PDF and the results given by the advection–diffusion–dispersion approximation can be easily distinguished from those given by the advection–diffusion approximation (dashed curve in figure 2(*b*)).

In the next section we examine the result of including voltage threshold and reset along with a lower inhibitory voltage boundary.

3.2.4. With voltage reset and (sticky) lower boundary. In section 3.2 we gave the evolution equation for our one-dimensional model:

$$\frac{\partial \rho_V}{\partial t}(v,t) = -\frac{\partial}{\partial v} J(v,t) + \delta(v - v_{\text{reset}}) J_U(\tau_{\text{ref}}, t). \tag{52}$$

Our one-dimensional model is obtained from the development in section 3.2.1 by restricting $V(t)$ to $\mathcal{E}_{\text{i}} \leqslant V(t) < v_{\text{th}}$ and assuming that the flux across v, $J(v,t)$, is given by (43) in the restricted domain after suitable modifications taking into account the absorbing boundary at v_{th} and the no-flux condition at $\mathcal{E}_{\text{i}}$. We emphasize that this procedure cannot be justified rigorously. It simply provides one method for obtaining a one-dimensional model for a truly high-dimensional stochastic process.

Inserting a lower voltage boundary at $v = \mathcal{E}_{\text{i}}$ makes $\rho_V(v,t) = 0$ for $v < \mathcal{E}_{\text{i}}$, and hence no contribution to the flux can be made by neurons with $V(t) < \mathcal{E}_{\text{i}}$. Thus the limits of integration for the excitatory flux (43) should be modified to reflect this voltage dependency:

$$J_{\text{e}}(v,t) = \int_{-\infty}^{t} \mathrm{d}t' h_{\text{e}}(t-t') v_{\text{e}}(t') \int_0^{\frac{V-\mathcal{E}_{\text{i}}}{q_{\text{e}}(t-t')}} \mathrm{d}x\, x f_{A_{\text{e}}}(x)\, \rho_V\big(v - x q_{\text{e}}(t-t'), t\big). \tag{53}$$

If we expand $\rho_V(v - x q_{\text{e}}(t-t'), t)$ in a Taylor series, then for our particular density function for A_{e} given in appendix A:

$$J_{\text{e}}(v,t) = \sum_{k=0}^{\infty} \frac{(-1)^k}{k!} \int_{-\infty}^{t} \mathrm{d}t' h_{\text{e}}(t-t') q_{\text{e}}^k(t-t') v_{\text{e}}(t') \mu_{A_{\text{e}}^{k+1}} \times \big(1 - F(q_{\text{e}}(t-t'); z, k)\big)\, \frac{\partial^k}{\partial v^k} \rho_V(v,t) \tag{54}$$

where $z = v - \mathcal{E}_{\text{i}}$, $F(q; z, k) = \mathrm{e}^{-\frac{z}{aq}} \sum_{l=0}^{n+k} \frac{1}{l!} \left(\frac{z}{aq}\right)^l$ and a is a parameter of the density function for A_{e} (see appendix A). We wish to compute the coefficients of $\frac{\partial^k \rho_V}{\partial v^k}$ in an efficient manner. When the unitary event waveform is a sum of exponentials or a gamma function, the convolution of $v(t)$ with $h(t)q^k(t)$ can be computed by updating a system of ODEs at each time step. The term $F(q_{\text{e}}(t-t'); z, k)$ in (54) stands in the way of this method, but this problem can be eliminated by expanding $F(q_{\text{e}}(t); z, k)$ in a Taylor series around the peak value of $q_{\text{e}}(t)$, $q_{\text{peak}} = \frac{\mu_{\text{EPSP,peak}}}{\mu_{A_{\text{e}}}}$:

$$F(q; z, k) \approx F(q_{\text{peak}}; z, k) + F'(q_{\text{peak}}; z, k)\big(q - q_{\text{peak}}\big). \tag{55}$$

In practice we find a zero-order Taylor series ($F(q(t); z, k) \approx F(q_{\text{peak}}; z, k)$) to be sufficient: that is, the contribution from including higher-order terms is negligible. Similar arguments can be made for the inhibitory flux.

Since the advection–diffusion–dispersion approximation involves three derivatives of the density function and we place a lower bound on the hyperpolarization level of a neuron, we need a total of six conditions on $\rho_V(v,t)$ for the domain $v > v_{\text{reset}}$ and the domain $v < v_{\text{reset}}$: (1) from conservation of probability, the flux across threshold is also the flux across the reset potential; (2) from the absorbing boundary at v_{th}, we find that that $\rho_V(v_{\text{th}}, t) = 0$; (3) by a local analysis at v_{th} one can self-consistently solve for the second v-derivative of $\rho_V(v,t)$ in terms of the first v-derivative; (4) $\rho_V(v^+_{\text{reset}}, t) = \rho_V(v^-_{\text{reset}}, t)$; (5) in order to incorporate a lower bound on the membrane potential, the flux at $\mathcal{E}_{\text{i}}$ is equal to zero and (6) we set $\frac{\partial \rho_V}{\partial v}|_{v=\mathcal{E}_{\text{i}}} = 0$. This is done for simplicity in our numerical method, and we consider this boundary condition to be part of our model. (A correct but unwieldy boundary condition at $v = \mathcal{E}_{\text{i}}$ can be found by a method analogous to that used at $v = v_{\text{th}}$. The flux at $v = \mathcal{E}_{\text{i}}$ is set equal to zero and then differentiated with respect to time. The time derivatives of ρ_V are then replaced by the

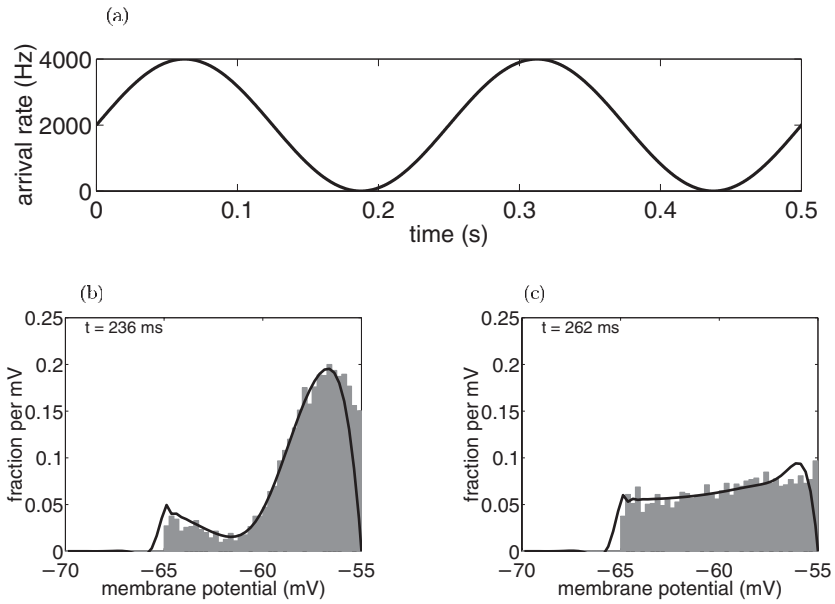

Figure 3. Snapshots of the PDF for a population responding to excitation only. (*a*) The arrival rate of excitation. (*b*) The PDF at $t = 236$ ms. (*c*) The PDF at 262 ms. Parameters: $\tau_e = 5$ ms and $\mu_{\text{EPSP,peak}} = 0.5$ mV. The voltage bin width in this and all following population density figures is 0.25 mV.

right-hand side of the conservation equation.) Details of these boundary conditions are given in appendix B.

The effects of adding these boundaries are illustrated by snapshots of the PDF in figures 3 and 4. In order to demonstrate the effects of threshold and reset, figures 3(*b*) and (*c*) show the PDF with only an excitatory current applied. Figure 3(*b*) shows the population at the onset of firing following a period of quiescence and figure 3(*c*) shows the population after it has been firing for a prolonged period. When the population is just starting to fire, we see a large buildup of neurons near the threshold and a small buildup near the reset. After a prolonged period of firing the neurons spread out fairly uniformly between the reset voltage and threshold. This latter result is consistent with the stationary distribution analytically found in Brunel and Hakim (1999) and modified in appendix C to take into account the refractory period. Note that our model PDF must be zero at threshold, but the histogram does not approach zero as v approaches v_{th}. In the actual random process realized by the Monte Carlo simulations, it is possible for neurons to be infinitesimally close to the threshold. In fact (19) shows that in the true random process, the firing rate $r(t)$ is proportional to the marginal density function evaluated at threshold, $\rho_V(v, t)$.

In order to demonstrate behaviour near the lower inhibitory boundary, figures 4(*b*)–(*e*) show the PDF with only inhibitory current. As the population approaches the lower boundary (figure 4(*b*)) there is good agreement between the population density method and Monte Carlo simulation. However, in figure 4(*c*) we see that once the Monte Carlo population builds up at this lower boundary, neurons in the one-dimensional model start to diffuse away from the boundary. This results in the population density model leading the Monte Carlo simulation in a return to rest as the inhibitory input diminishes (figure 4(*d*)). Once the neurons near the resting potential, the model and simulation return to strong agreement, as shown in figure 4(*e*).

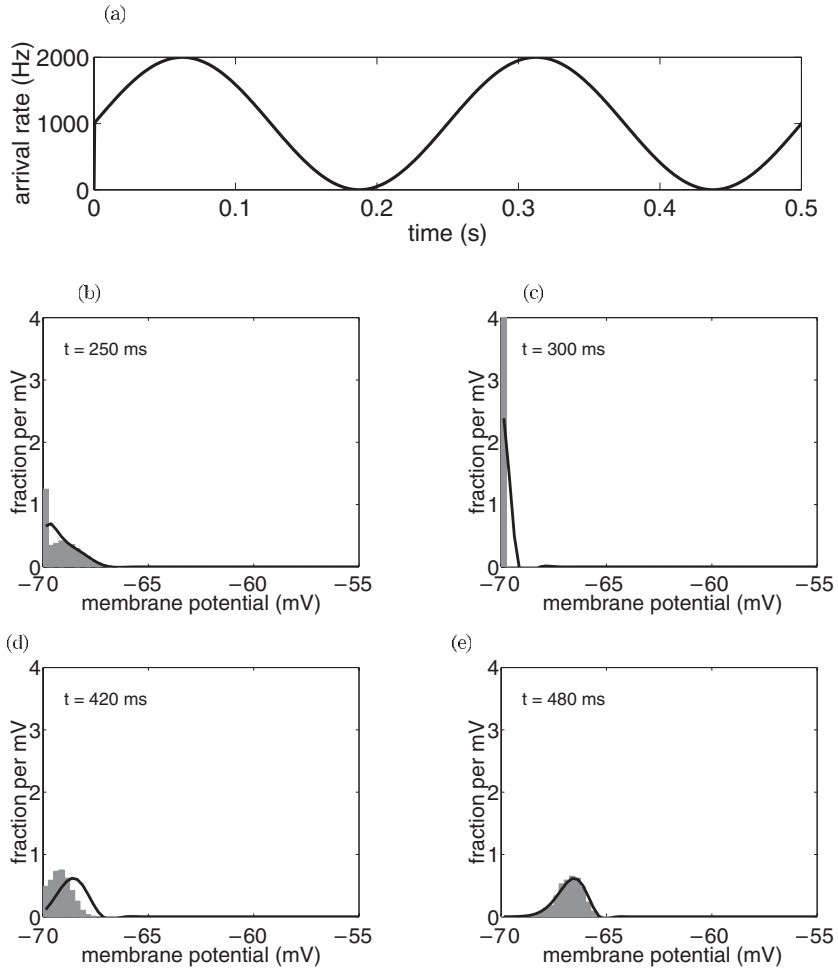

Figure 4. Snapshots of the PDF for a population responding to inhibition only. (*a*) The arrival rate of inhibition. (*b*)–(*e*) Show the PDF at $t = 250$, 300, 420 and 480 ms respectively (0.25 mV bin width). Parameters: $\tau_i = 10$ ms and $\mu_{\mathrm{IPSP,peak}} = 0.25$ mV.

4. Single-population simulations

In this section we examine the population response with various different parameters and driving forces. The population density method developed in the previous section will be compared with Monte Carlo simulations of a large population of individual integrate-and-fire neurons and with results from mean-field theory. Since the Monte Carlo simulations are of the original SDE (1), the Monte Carlo simulations are considered to be correct in the sense that, by the law of large numbers, they converge to the average result as the population size N approaches infinity.

We emphasize that in our demonstrations the single-neuron parameters were chosen such that our three-term truncated Taylor series approximation for the integrand in the partial differential-integral equation (52) is excellent. Thus, the discrepancies between our population density results and Monte Carlo results stem from the one-dimensional model and not from the Taylor series approximation.

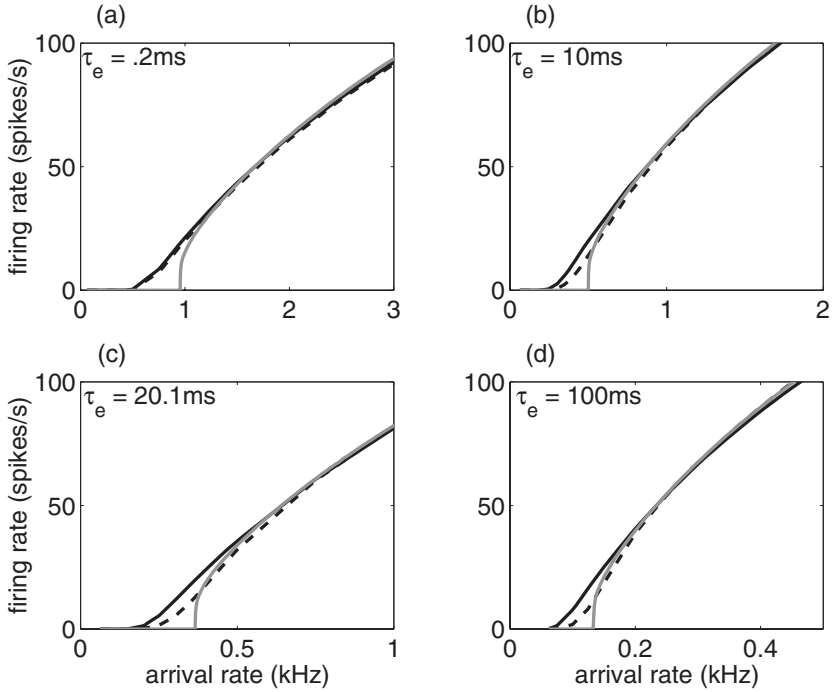

Figure 5. The relationship between firing rate and the arrival rate of unitary excitatory synaptic events. The results from mean-field theory (grey curve), population density method (dark curve) and Monte Carlo simulations (dashed curve) are compared. In each panel, the synaptic time constant for decay is given. In all panels, $\mu_{\mathrm{EPSP,peak}} = 0.5$ mV.

4.1. Steady-state analysis

In figure 5 the performance of our one-dimensional model is examined when a single uncoupled population of neurons receives Poisson excitatory input at various steady prescribed rates. In the case of very fast synaptic kinetics, shown in figure 5(*a*), there is near-perfect agreement between the one-dimensional model (dark curve) and direct Monte Carlo simulation (dashed curve). This is not surprising, since the random process is truly one-dimensional in the limit of instantaneous synaptic kinetics (Nykamp and Tranchina 2000). With slow synaptic kinetics, the agreement between Monte Carlo and population density results is still very good at high firing rates, but the model tends to overestimate low firing rates, as shown in figures 5(*b*)–(*d*). The discrepancies between Monte Carlo and our one-dimensional model in the regime of low firing rates become somewhat more pronounced as the synaptic kinetics are made slower. Note that the threshold for the onset of firing in the mean field (grey curve) is sharp and much higher than the location of the foot of the Monte Carlo curve (dashed curve). Thus, the mean-field method badly underestimates low firing rates. At the threshold of firing onset for the mean field the slope of the input–output relationship is infinite, unlike that of the Monte Carlo simulation and population density method.

The model results in figure 5 were computed with the advection–diffusion–dispersion approximation, but for the EPSP size distribution used in this illustration, the advection–diffusion results (not shown) are similar. The steady-state advection–diffusion problem can be solved analytically (Brunel and Hakim 1999), and we provide the solution in appendix C with the refractory period taken into account. As a further check of our numerical methods,

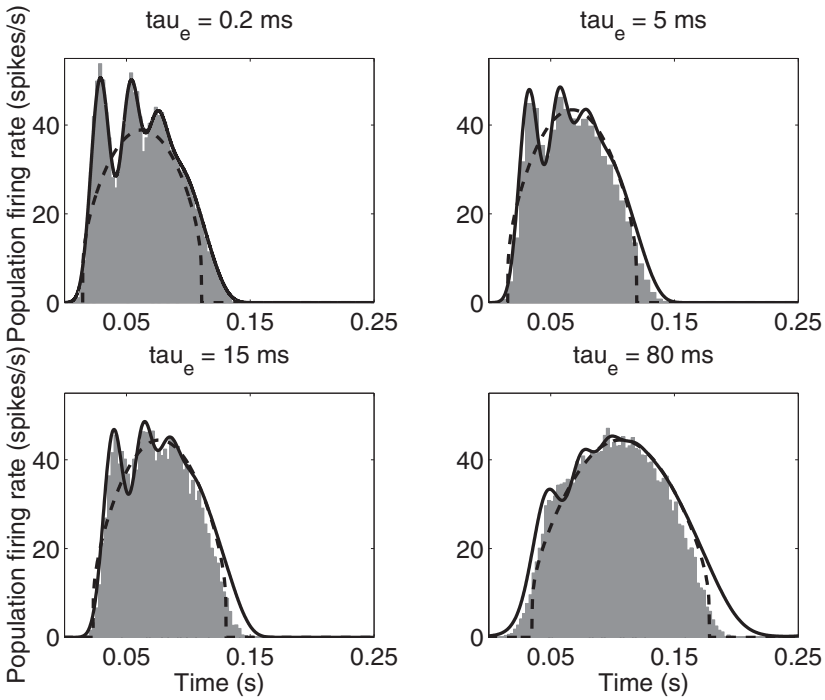

Figure 6. The population response to excitation modulated by a 4 Hz sinusoid is shown for one period of stimulation. Monte Carlo simulation (histogram) is compared to the advection–diffusion–dispersion (solid curve) and mean-field (dashed curve) results. The synaptic time constant of decay is given in each panel. The mean arrival rate of excitation is varied to maintain an approximate peak firing rate of 40–45 Hz. $\mu_{\mathrm{EPSP,peak}} = 0.25$ mV for all figures.

we compared our numerical solution for the steady-state advection–diffusion problem with the analytical solution and found them to be indistinguishable (not shown).

4.2. Dynamic stimulus response

In figure 6, we show the response to excitation modulated by a single 4 Hz sinusoid for various different time constants of decay for the single-exponential unitary post-synaptic current event. Each panel contains one period of stimulation. There is excellent *qualitative* agreement between the advection–diffusion–dispersion approximation (solid curve) and Monte Carlo simulation (histogram) for synaptic time constants that are both fast and slow compared with the membrane time constant. However, as the synaptic time constant increases, the quantitative agreement breaks down toward the end of the period. The strong agreement for very fast synaptic kinetics in figure 6(*a*) is consistent with Nykamp and Tranchina (2000). Quantitative agreement for the case where $\frac{\tau_e^d}{\tau_m} = 0.25$ in figure 6(*b*) is still quite good. This result is not peculiar to the particular stimulus in figure 6, as can be seen from figures 9 and 10. Note that our one-dimensional population density model does a good job of capturing the smeared-out phase locking (population synchrony) exhibited by the Monte Carlo simulation. The tendency of integrate-and-fire neurons to phase lock with periodic modulation of synaptic current or conductance is a well known phenomenon (Knight 1972). In our simulations the synaptic noise causes dispersion in the firing times.

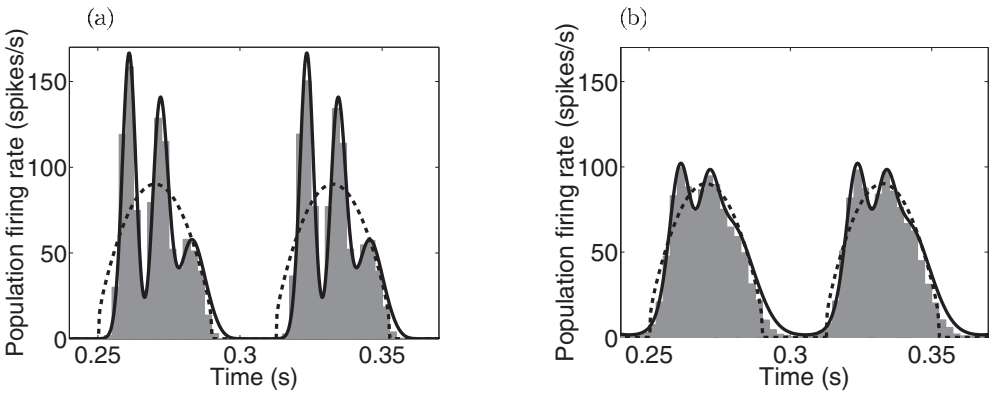

Figure 7. The response of a population of neurons to 16 Hz sinusoidally modulated excitatory input. The results from mean-field theory (dashed curve), population density method (solid curve), and Monte Carlo (histogram) are compared. (*a*) Response to excitation modulated by a 16 Hz sine wave at a mean arrival rate of 2000 Hz. (*b*) As (*a*), but with an additional 2000 Hz of constant excitation balanced by 2000 Hz of constant inhibition. Parameters: $\tau_e = 5$ ms, $\tau_i = 5$ ms, $\mu_{EPSP,PEAK} = 0.25$ mV, $\mu_{IPSP,PEAK} = 0.25$ mV.

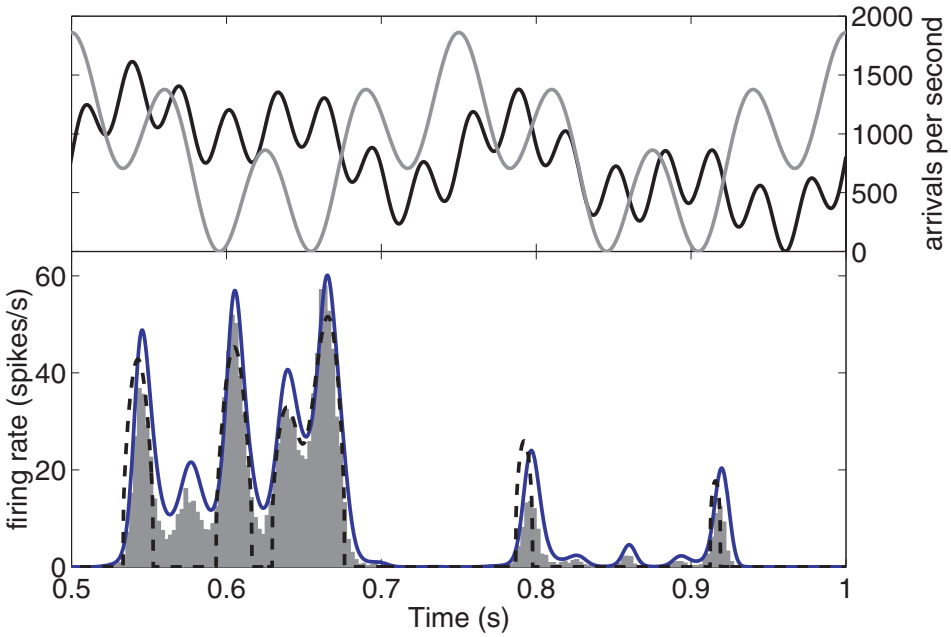

Figure 8. The response of a population of neurons to a dynamically rich excitatory and inhibitory input. The results from mean-field theory (dashed curve), population density method (solid curve), and Monte Carlo (histogram) are compared in the bottom panel. The top panel shows the arrival rate of excitation (dark curve) and inhibition (grey curve). Parameters: $\tau_e = 5$ ms, $\tau_i = 10$ ms, $\mu_{EPSP,peak} = 0.5$ mV, $\mu_{IPSP,peak} = 0.25$ mV.

Figure 7 shows another response feature that is captured by the population density method but not by the mean field method: sensitivity to the addition of perfectly balanced excitation and inhibition. Figure 7(*a*) shows the population response to Poisson input in which the

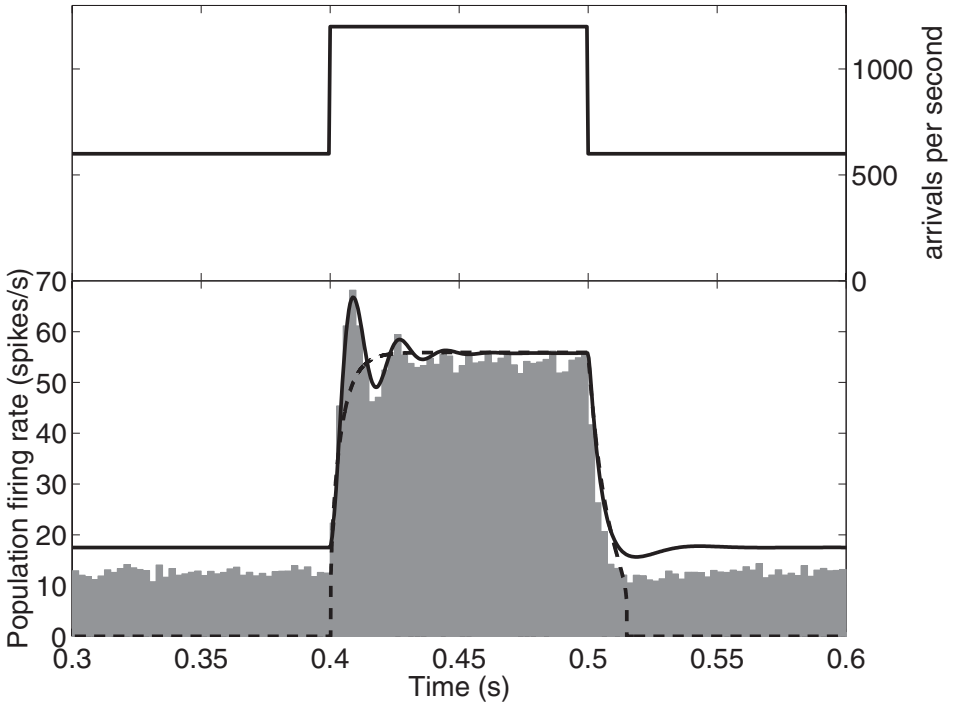

Figure 9. The response to a step increase in the arrival rate of excitation shown in the top panel is displayed in the bottom panel. Monte Carlo simulation (histogram) is compared to the advection–diffusion–dispersion approximation (solid curve) and mean-field (dashed curve) results. Parameters: $\tau_e = 5$ ms, $\mu_{EPSP,peak} = 0.5$ mV.

rate of excitatory events is modulated by a single sinusoid at 16 Hz (two stimulus periods are shown). The population density method (solid curve) is compared to both Monte Carlo simulations (histogram) and mean-field results (dashed curve). Notice that the population density method again captures the population synchrony exhibited by Monte Carlo simulation. The mean-field method is not capable of capturing this dynamic property. Figure 7(*b*) is the same as 7(*a*) except that a constant arrival rate of 2000 synaptic events per second is added to both the excitatory and inhibitory input. Since the parameters of the excitatory synapses and inhibitory synapses were chosen to be the same, this added input leaves the advection and dispersion terms unchanged but increases the diffusion term. This increase in the diffusion term represents an increase in the noise of the input. Comparing the two figures, one sees that the average firing rate of the population remains about the same; however, the firing rate function has been smoothed. Since there is an increased level of synaptic activity and much less dynamical behaviour in the firing rate, the mean-field approximation appears to perform much better in this setting. However, the remaining dynamical behaviour and periods of low firing are still captured better overall by the population density method (advection–diffusion–dispersion approximation).

Figure 8 shows typical performance of our population density method when a population is simultaneously driven by fast excitatory input ($\tau_e = 5$ ms) and slower inhibitory input ($\tau_i = 10$ ms). In this illustration the excitatory and inhibitory input rates are modulated independently by sums of sinusoids in order to generate a temporally rich stimulus. The

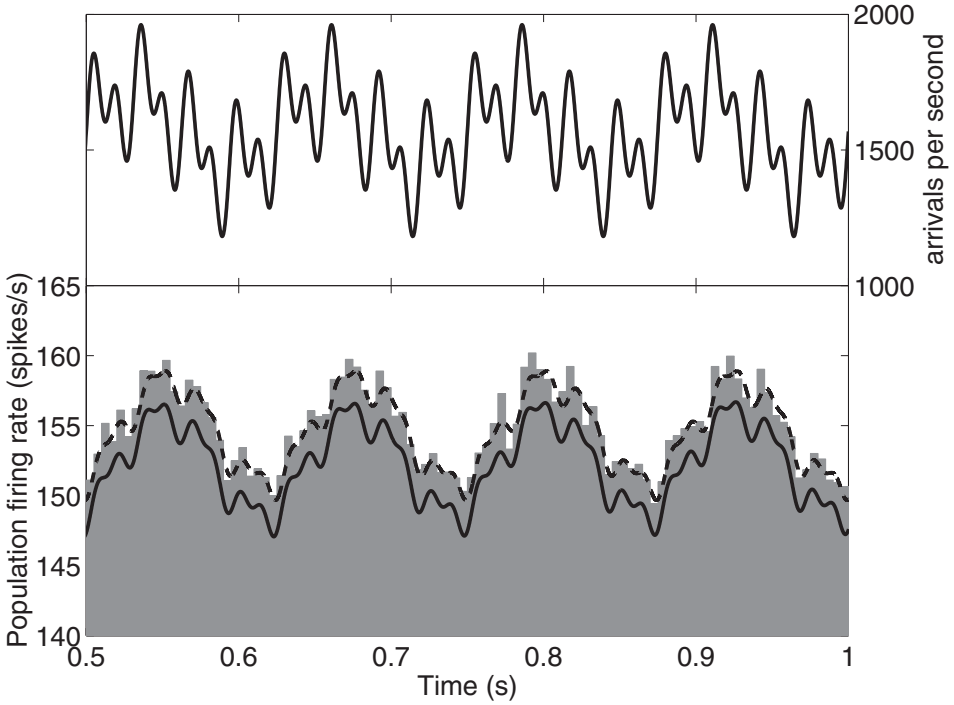

Figure 10. The PDF method performs well in the regime of small perturbations around a high mean firing rate regardless of the synaptic time constant. The maximum and minimum arrival rate differ from the mean arrival rate by 24.83%, as shown in the top panel. Monte Carlo simulation (histogram) is compared with the advection–diffusion–dispersion approximation (solid curve) and mean-field (dashed curve) results in the bottom panel. Parameters: $\tau_e = 40$ ms, $\mu_{EPSP,peak} = 0.5$ mV.

population density method (solid curve) consistently overestimates low firing rates. These discrepancies result largely from the slow inhibition with $\frac{\tau_i^d}{\tau_m} = 0.5$. Note, however, that the population density method does a good job of capturing the temporal structure in the Monte Carlo results (histogram). The mean-field method (dashed curve) misses some periods of activity completely.

Figure 9 shows the population response to a step increase in the arrival rate of excitation. Due to a substantial fraction of neurons near threshold before the step onset there is a strong initial response to the onset of the transient which is captured well by the population density method. This damped oscillatory approach of the population firing rate to a new equilibrium is similar to that illustrated in Gerstner (1999) and Nykamp and Tranchina (2000); it has recently been treated analytically (Knight *et al* 2000). The mean-field method assumes all neurons are starting from v_{reset} and receiving the same constant current; hence, it misses this fast transient, and the smooth temporal structure of the mean-field response simply reflects the dynamics of the mean excitatory current. Prior to the transient the population is at a steady firing rate of 13 Hz. The advection–diffusion–dispersion approximation overestimates this as 17 Hz and the mean-field method reports no firing.

Figure 10 shows that our PDF method performs well in the regime of small perturbations in the firing rate around a high mean level even when the synaptic kinetics are slow. In this simulation, $\frac{\tau_e}{\tau_m} = 2$. Although the population density method does tend to underestimate the

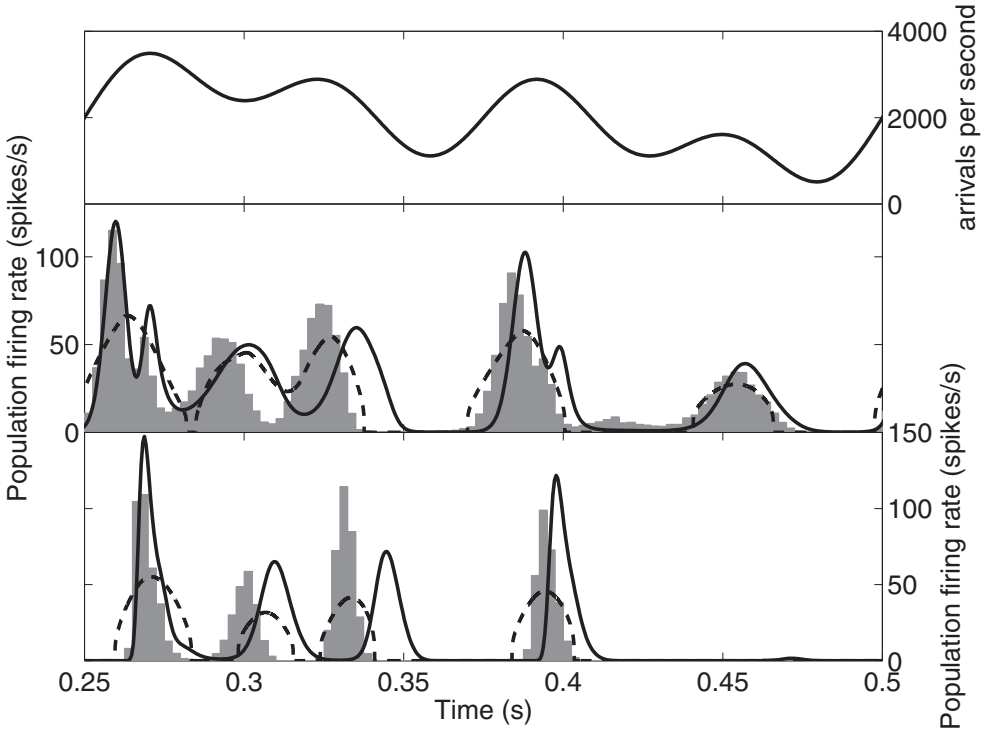

Figure 11. The excitatory arrival rate displayed in the top panel is delivered to an excitatory population shown in the middle panel. The bottom panel is the inhibitory population. Here each population is supplying on average 40 synapses per neuron to the other population. Results from Monte Carlo (histogram) are compared with the population density method (solid curve) and mean field (dashed curve). Parameters: $\tau_e = 5$ ms, $\tau_i = 10$ ms, $\mu_{EPSP} = 0.25$ mV, $\mu_{IPSP} = 0.25$ mV, and mean synaptic delay, $\bar{\alpha} = 3$ ms.

Monte Carlo result more so than the mean-field theory, these differences are very small on the order of the Monte Carlo firing rate.

5. Interacting populations

We now turn the focus to interacting populations. In this setting a separate PDF, $\rho_v^k(v, t)$, is evolved for each population, $k = 1, 2, \ldots, N$. When populations are coupled together, the arrival rates of excitatory/inhibitory unitary synaptic events $\nu_{e/i}$ are determined by the rate of external input and the firing rates of the various presynaptic populations:

$$\nu_{e/i}^k(t) = \nu_{e/i,o}^k(t) + \sum_j w_{jk} \int_0^\infty \alpha_{jk}(t') r^j(t - t')\, dt', \tag{56}$$

where $\nu_{e/i,o}$ is the arrival rate of events originating from external input, w_{jk} is the average number of synapses a neuron in population k receives from population j, and $\alpha_{jk}(t)$ is the distribution of synaptic latencies from population j to population k.

The simulations below involve two interacting populations, one excitatory and one inhibitory, with external input to the excitatory population only. In the Monte Carlo simulations, each population consists of 1000 neurons, and the results are averaged over five realizations of

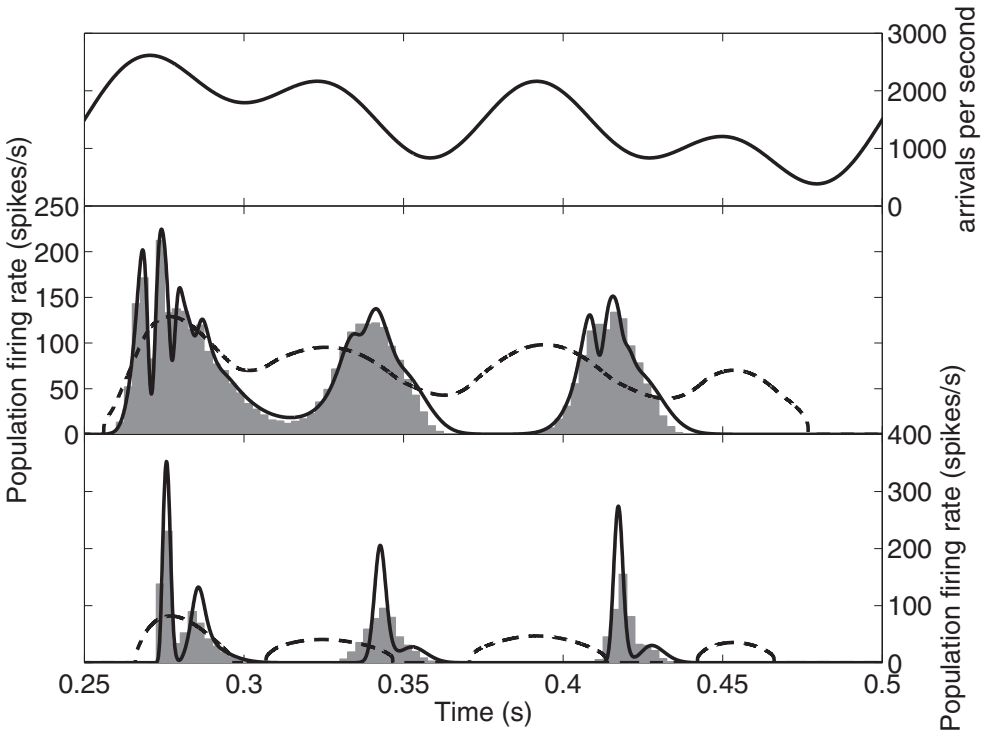

Figure 12. The excitatory arrival rate displayed in the top panel (the same as that in figure 11) is delivered to an excitatory population shown in the middle panel. The bottom panel is the inhibitory population. Here each population supplies on average 50 synapses per neuron to itself and the other population. Results from Monte Carlo (histogram) are compared with the population density method (solid curve) and mean field (dashed curve). The temporal structure of the mean-field response is grossly incorrect. Parameters: $\tau_m = 20$ ms, $\tau_e = 5$ ms, $\tau_i = 22$ ms, $\mu_{\mathrm{EPSP,peak}} = 0.25$ mV, $\mu_{\mathrm{IPSP,peak}} = 0.25$ mV, $\bar{\alpha} = 3$ ms.

the random network connectivity. The distribution of synaptic latencies are given by a ninth-order ($n = 9$) gamma distribution with a mean of 3 ms. This is similar to the synaptic latency distribution used by Somers *et al* (1995) and the same as used by Nykamp and Tranchina (2000). The same synaptic latency distribution is utilized for each connection.

5.1. Two-population simulations

When an excitatory and an inhibitory population are coupled together, some of the deficiencies of the one-dimensional model can become more pronounced. However, we demonstrate, with a few typical examples, that on the whole the population density method does a much better job of capturing network activity than the mean-field method.

In figure 11, the excitatory population receives an external excitatory input at an average rate of 2000 arrivals per second modulated by a temporally rich sum of sinusoids. The excitatory population feeds forward to the inhibitory population with an average coupling of 40 synapses per neuron. The inhibitory population feeds back into the excitatory population with an average coupling of 40 synapses per neuron. Figure 11 shows that the population density method (solid curve) has some timing difficulties, but the times of peak activity differ from those in the Monte Carlo simulations (histogram) by less than 15 ms. The population density method also misses

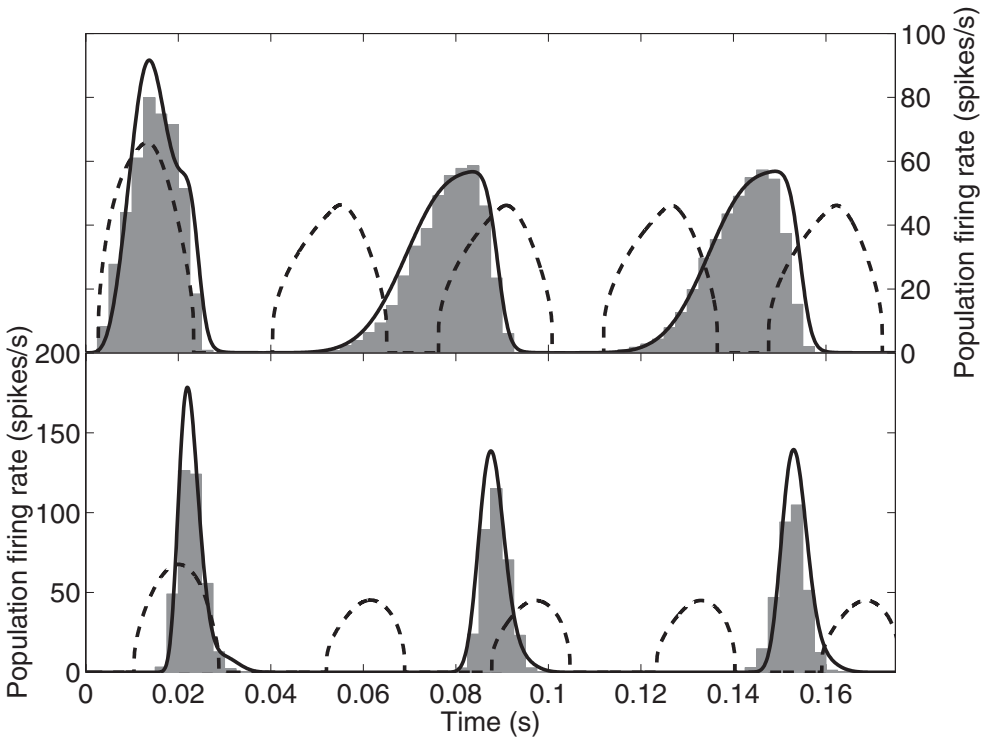

Figure 13. Network oscillations under steady input conditions in coupled populations of excitatory and inhibitory neurons with slow inhibition. A constant 1500 Hz arrival rate of excitatory events is applied to an excitatory population shown in the top panel. The bottom panel is the inhibitory population. Here each population supplies on average 50 synapses per neuron to the other population. Results from Monte Carlo (histogram) are compared with the population density method (solid curve) and mean field (dashed curve). This network architecture with the parameters below creates oscillations in the population response to a steady external input. The population density and Monte Carlo results match fairly well. The mean-field method gives oscillatory activity but at the wrong frequency. Parameters: $\tau_m = 20$ ms, $\tau_e = 5$ ms, $\tau_i = 22$ ms, $\mu_{\mathrm{EPSP,peak}} = 0.25$ mV, $\mu_{\mathrm{IPSP,peak}} = 0.25$ mV, $\bar{\alpha} = 3$ ms.

some periods of very low firing. The performance of the mean-field approach in this particular simulation is comparable to that for uncoupled populations above.

The simulation of a 500 ms stimulus–response period in figure 11 required 2.3 s for the population density method and 289 s to average five Monte Carlo simulations of the random network (using a Silicon Graphics computer with a 250 MHz MIPS R10000 processor).

Figure 12 shows a simulation in which each population supplies on average 50 synapses per neuron to itself and the other population. The excitatory population (middle panel) receives the same external input as in figure 11. There are sharp peaks of activity, particularly around 275 ms, corresponding to population synchrony. Since the firing rate is computed by population averaging rather than temporal averaging, the high peak firing rates are from a large number of neurons firing in a short time period rather than individual neurons firing at an extremely high rate. The mean-field method performs temporal averaging, and therefore it cannot capture this population synchrony. In general, the mean-field method performs rather poorly for this example; the temporal structure of the mean-field firing rate is grossly incorrect for both the excitatory and inhibitory population. The population density method does a much better job of capturing the network activity.

For some choices of network architecture and synaptic kinetics, network oscillations can be achieved by applying a constant excitation. An example of this is shown in figure 13. Here an excitatory population receiving constant external input feeds forward onto an inhibitory population that then feeds back to the excitatory population. There are an average of 50 synapses made per neuron. In the excitatory population, the period between oscillations is of the order of the firing duration of the inhibitory population. Once the inhibition shuts down the excitatory population, the inhibitory population no longer receives excitation. This in turn shuts down the inhibitory population, allowing the excitatory population to resume firing and the cycle to start over again. There is a fairly good match between population density and Monte Carlo results in this example. The mean-field method does give network oscillations but at a frequency that is far off.

6. Discussion and conclusion

Until recently, probability density or population density methods have been used primarily as a tool to study the statistics of random spike trains (Tuckwell 1988, Wilbur and Rinzel 1982, 1983). Beginning about 10 years ago, population methods have been used to obtain results on activity in networks of neurons (Abbott and van Vreeswijk 1993, Brunel and Hakim 1999, Strogatz and Mirollo 1991, Kuramoto 1991, Barna, Gröbler and Érdi 1998, Treves 1993, Chawanya *et al* 1993, Adorján *et al* 1999, Knight *et al* 2000, Nykamp and Tranchina 2000, Pham *et al* 1998, Gerstner and van Hemmen 1994, Gerstner 1995, 1999).

Although population density methods seem promising and may provide time-saving alternatives to conventional direct simulations, these methods do present their own difficulties. One stems from the fact that the incorporation of realistic synaptic kinetics into the underlying single-neuron model gives a high-dimensional population density function. A post-synaptic conductance whose unitary event time course is a simple difference-of-exponentials (or alpha function), for example, adds two dimensions to the PDF. When the dimension of the population density function is greater than one or two at the most, it becomes more time consuming to compute network activity by the population density method than by the conventional direct method.

It has been shown previously that when the excitatory synapse is modelled as instantaneous and the inhibitory synapse is non-instantaneous, a mean-field approximation on the inhibitory conductance random variable gives good results in the presence of sufficient excitation. This mean-field approximation on the inhibitory conductance retains a one-dimensional population density function. This method would not work, however, with an intrinsically oscillatory underlying neuron which is driven by inhibition only. Furthermore, in cases where there is both excitatory and inhibitory input, excitatory conductances gated by AMPA or kainate receptors are often not sufficiently fast on the time scale of the membrane time constant to be well approximated as instantaneous. Excitatory conductances gated by the NMDA-type of ionotropic receptors or by metabotropic receptors are particularly slow. These facts motivated our attempt to develop computationally efficient population density methods that can handle arbitrary synaptic kinetics. Our method is based on the simple idea that the firing rate of a population of integrate-and-fire neurons is given by the total flux of probability across the threshold voltage. Therefore, the firing rate is determined by the evolution equation for the marginal density function, $\rho_V(v,t)$. We showed that an exact evolution equation for $\rho_V(v,t)$ can be written for a simple, related, but artificial, stochastic process, in which synaptic input is modelled as current injection and both voltage reset and the lower bound on voltage (at the reversal potential for inhibitory post-synaptic current for a conductance-driven neuron) are eliminated. The derivation of the one-dimensional evolution equation for this stochastic

process relies on the fact that, in this process, the membrane potential is a linear functional of the synaptic currents. This is no longer the case when voltage is reset after neurons cross threshold.

Our one-dimensional model for the integrate-and-fire neuron was obtained by using, without rigorous justification, the evolution equation for the simpler stochastic process and by adding appropriate boundary conditions. The resulting evolution equation is a partial differential-integral equation, and it is exactly correct in the limit of instantaneous synaptic kinetics; in the instantaneous synapse case, the stochastic process is truly a one-dimensional Markov process. Consequently, one would expect our model to give good results for fast (but non-instantaneous) synaptic kinetics, and we showed that this is indeed the case. Unfortunately, performance degenerates as the synaptic kinetics are made slower and slower.

The discrepancies between our one-dimensional model and Monte Carlo simulations are evident both for steady and dynamic stimuli; the one-dimensional model overestimates low firing rates. The one-dimensional model does a very good job of capturing moderate modulations in firing rate around some moderate-to-high mean firing rate regardless of synaptic time constants. Under dynamic stimulus conditions, the one-dimensional model generally does a good job of matching the times of the peaks and troughs in activity, but sometimes misses substantially the magnitudes at these points for large synaptic time constants. Deficiencies of the one-dimensional model can be more pronounced when populations are coupled together (figure 11).

The mean-field method, on the other hand, underestimates low firing rates in the steady state, and has a sharp threshold synaptic current for the onset of firing. The mean-field method cannot capture periods of high population synchrony. Mean-field results can be grossly incorrect when an excitatory and an inhibitory population are coupled together (figures 12 and 13).

An alternative to the one-dimensional model as a method for reducing the dimension of the probability density problem to be solved is a moment-expansion method, which gives systems of coupled partial differential equations and auxiliary ODEs for each population. The method was described briefly by Nykamp and Tranchina (2001) in connection with slow inhibition. In order to describe the method, we focus on the case of excitatory synaptic current injection only, in which the unitary synaptic event waveform is a single exponential. In this case, the PDF is two-dimensional with arguments v (voltage), x (synaptic current divided by membrane capacitance) and t (time). From the conservation equation for this system, a series of partial differential equations can be obtained by multiplying through by x^k and integrating over x. Let us define $f_V^{(k)}(v,t) = \mu_{X^k|V}(v,t)\rho_v(v,t)$, where $\mu_{X^k|V}(v,t)$ is the kth moment of X given V, and $f_V(v,t)$ is the marginal PDF for V. The series of partial differential equations relate each $f_V^{(k)}$ to all lower terms (i.e. $f_V^{(j)}$ for $j = 1, 2, \ldots, k-1$) and to the next-higher term, $f_V^{(k+1)}$. The firing rate for this system is determined by $f_V^{(0)}$ and $f_V^{(1)}$. One method to obtain an approximate solution for the various $f_V^{(k)}$ up to some level, say $k = n$, is to make the approximation that the centred $n+1$ moment of X is independent of V. An ODE for any unconditioned moment of X is easily obtained from the stochastic ODE describing the evolution of X. It is possible that stopping at the level $k = 1$ will give good approximate results. In this case, the approximation that the variance of X is independent of V would be made, and only two coupled partial differential equations would result. Two coupled one-dimensional partial differential equations could be solved in far less time than one two-dimensional partial-differential-integral equation.

We view our one-dimensional model as a first attempt at dealing with the dimension problem caused by the introduction of realistic synaptic kinetics in the population density

framework. Our methods give results that are more accurate than those of the mean-field method, but there is certainly room for improvement. The method appears to be good enough to use in the exploration of parameter space in testing neuronal network models, but final testing of a promising model should still probably be done with direct simulation.

Appendix A. Parameters

The following parameters were used for all simulations: $\mathcal{E}_{\mathrm{i}} = -70$ mV, $\mathcal{E}_{\mathrm{r}} = v_{\mathrm{reset}} = -65$ mV, $v_{\mathrm{th}} = -55$ mV, $\mathcal{E}_{\mathrm{e}} = 0$ mV, $\tau_m = 20$ ms and $\tau_{\mathrm{ref}} = 3$ ms.

The sizes of the unitary synaptic events are given according to a gamma distribution with density

$$f_{A_{\mathrm{e/i}}}(x) = \frac{\exp(-x/a_{\mathrm{e/i}})}{a_{\mathrm{e/i}}(n_{\mathrm{e/i}}-1)!}\left(\frac{x}{a_{\mathrm{e/i}}}\right)^{n_{\mathrm{e/i}}-1}, \tag{57}$$

where $f_{A_{\mathrm{e/i}}}$ is the PDF for $A_{\mathrm{e/i}}$. The average values of $A_{\mathrm{e/i}}$ were chosen to provide a prescribed average peak membrane potential change to a unitary synaptic event. The coefficient of variation was chosen to be 0.5. The mean and coefficient of variation determine the parameters $a_{\mathrm{e/i}}$ and $n_{\mathrm{e/i}}$.

For simulations involving interacting populations, the distribution of synaptic latencies were given by a ninth-order ($n = 9$) gamma distribution with a mean of 3 ms ($a = \frac{1}{3}$ ms). The same synaptic latency distribution was used for each connection.

Appendix B. Boundary conditions

The probability that the membrane potential is in the interval $(v - \Delta v, v)$ can be approximated by

$$\Pr\{V(t) \in (v-\Delta v, v)\} = \rho_V(\xi, t)\Delta v + \mathrm{O}((\Delta v)^2), \qquad \text{for} \quad v - \Delta v < \xi < v. \tag{58}$$

Let us consider the time evolution of this area at $v = v_{\mathrm{th}}$ when there are no externally applied forces. The only force acting on the neuron is leakage, which is zero at threshold since no neuron may contribute to the flux from above v_{th}:

$$\frac{\partial}{\partial t}\rho_V(\xi, t)\Delta v = -(\text{flux in} - \text{flux out}) \tag{59}$$

$$= J_l(v_{\mathrm{th}} - \Delta v, t) - J_l(v_{\mathrm{th}}, t) \tag{60}$$

$$= -\frac{1}{\tau_m}(v_{\mathrm{th}} - \Delta v - \mathcal{E}_{\mathrm{r}})\,\rho_V(v_{\mathrm{th}} - \Delta v, t) - 0. \tag{61}$$

Now we expand $\rho_V(v_{\mathrm{th}} - \Delta v, t)$ in a Taylor series—the v-derivative of $\rho_V(v, t)$ evaluated at v_{th} are to be interpreted as one-sided derivatives taken from below v_{th}:

$$\frac{\partial}{\partial t}\rho_V(\xi, t) = -\frac{1}{\tau_m}(v_{\mathrm{th}} - \Delta v - \mathcal{E}_{\mathrm{r}})\,\frac{1}{\Delta v}\left[\rho_V(v_{\mathrm{th}}, t) - \frac{\partial \rho_V}{\partial v}\Big|_{v=v_{\mathrm{th}}}\Delta v + \mathrm{O}((\Delta v)^2)\right]. \tag{62}$$

Lastly, we ask what happens as Δv approaches zero:

$$\frac{\partial}{\partial t}\rho_V(v_{\mathrm{th}}, t) = -\frac{1}{\tau_m}(v_{\mathrm{th}} - \mathcal{E}_{\mathrm{r}})\left[\lim_{\Delta v \to 0}\frac{\rho_V(v_{\mathrm{th}}, t)}{\Delta v} - \frac{\partial \rho_V}{\partial v}\Big|_{v=v_{\mathrm{th}}}\right]. \tag{63}$$

In order for the above expression to make sense, it must be that the density is identically zero at threshold.

Now, given that $\rho_V(v_{\rm th}, t) = 0$, we seek to find a relationship between the first and second v-derivatives of $\rho_V(v, t)$ at the threshold boundary $v_{\rm th}$. Since there is no inhibitory flux at the $v_{\rm th}$ we consider the case of only an excitatory flux and begin with the evolution equation (20):

$$\frac{\partial \rho_V}{\partial t}(v_{\rm th}, t) = -\frac{\partial}{\partial v} J(v, t)\Big|_{v_{\rm th}} + \delta(v_{\rm th} - v_{\rm reset}) J_U(\tau_{\rm ref}, t) \tag{64}$$

$$= -\frac{\partial}{\partial v}\left[-\frac{1}{\tau_m}(v - \mathcal{E}_{\rm r})\rho_V(v, t) + J_{\rm e}(v, t)\right]_{v=v_{\rm th}} \tag{65}$$

$$= \frac{1}{\tau_m}\rho_V(v_{\rm th}, t) + \frac{1}{\tau_m}(v_{\rm th} - \mathcal{E}_{\rm r})\frac{\partial \rho_V}{\partial v}\Big|_{v=v_{\rm th}} + \frac{\partial J_{\rm e}}{\partial v}\Big|_{v=v_{\rm th}}. \tag{66}$$

We replace $J_{\rm e}(v, t)$ with the first three terms of the Taylor series approximation (54):

$$\frac{\partial}{\partial v} J_{\rm e}\Big|_{v=v_{\rm th}} = \left[(h * \nu)(t)\mu_A \frac{\partial \rho_V}{\partial v} - (qh * \nu)(t)\mu_{A^2}\frac{\partial^2 \rho_V}{\partial v^2}\right]_{v=v_{\rm th}}. \tag{67}$$

Now, since the density is constant at $v_{\rm th}$, we have that $\frac{\partial \rho_V}{\partial t}(v_{\rm th}, t) = 0$, which yields the relationship at $v_{\rm th}$:

$$\frac{\partial^2 \rho_V}{\partial v^2}\Big|_{v=v_{\rm th}} = \frac{\mu_A (h * \nu)(t) - \frac{1}{\tau_m}(v_{\rm th} - \mathcal{E}_{\rm r})}{\mu_{A^2}(qh * \nu)(t)} \frac{\partial \rho_V}{\partial v}\Big|_{v=v_{\rm th}}. \tag{68}$$

Appendix C. Analytic solution for diffusion approximation in steady state

The steady-state solution for the diffusion approximation has been provided by Brunel and Hakim (1999). We modify their solution below to take into account the refractory period, $\tau_{\rm ref}$. For the sake of simplified notation, we consider the case of excitatory input only. The addition of inhibitory input would simply change the advection and diffusion coefficients. The evolution equation for $\rho_V(v, t)$ in the diffusion approximation is

$$\frac{\partial \rho_V}{\partial t} = -\frac{\partial}{\partial v}\left\{\left[-\frac{1}{\tau_m}(v - \mathcal{E}_{\rm r}) + c_1 a(t)\right]\rho_V(v, t) + 2c_2 D(t)\frac{\partial \rho_V}{\partial v}\right\} + \delta(v - \mathcal{E}_{\rm r}) r(t - \tau_{\rm ref}). \tag{69}$$

In the steady state we have

$$0 = -\frac{\partial}{\partial v}\left\{\left[-\frac{1}{\tau_m}(v - \mathcal{E}_{\rm r}) + c_1 a\right]\rho_V(v) + 2c_2 D\frac{\partial \rho_V}{\partial v}\right\} + \delta(v - \mathcal{E}_{\rm r}) r. \tag{70}$$

Equation (70) implies that the total flux (the term in curly brackets) is constant for $\mathcal{E}_{\rm r} \leqslant v \leqslant v_{\rm th}$ and also for $\mathcal{E}_{\rm i} \leqslant v \leqslant \mathcal{E}_{\rm r}$, with a jump of r at $v = \mathcal{E}_{\rm r}$. The flux at $v_{\rm th}$ is the firing rate, r. Therefore, the constant flux to the right of $\mathcal{E}_{\rm r}$ is r, and to the left of $\mathcal{E}_{\rm r}$ is zero. The solutions for the two domains, $\mathcal{E}_{\rm r} \leqslant v \leqslant v_{\rm th}$ and $\mathcal{E}_{\rm i} \leqslant v \leqslant \mathcal{E}_{\rm r}$, can be combined into a single expression (Brunel and Hakim 1999):

$$\rho_V(v) = \frac{r}{2c_2 D}\exp\left[-\frac{1}{2\tau_m(2c_2 D)}(v - \mathcal{E}_{\rm r} - c_1 a\tau_m)^2\right] \times \int_v^{v_{\rm th}} H(v' - \mathcal{E}_{\rm r})\exp\left[\frac{1}{2\tau_m(2c_2 D)}\left(v' - \mathcal{E}_{\rm r} - c_1 a\tau_m\right)^2\right] {\rm d}v', \tag{71}$$

where $H(x)$ is the Heaviside step function.

Equation (71) contains the unknown firing rate, r. It is found by using the fact that the fraction of unrefractory neurons plus the fraction of refractory neurons is equal to 1. The fraction in the refractory state is given by $r\,\tau_{\rm ref}$. Thus, the firing rate is given by

$$r = \frac{-2c_2 D}{I - 2c_2 D\tau_{\rm ref}}, \tag{72}$$

where

$$I = \int_{\mathcal{E}_r}^{v_{th}} \mathrm{d}v \, \exp\left[-\frac{1}{2\tau_m(2c_2D)}\,(v - \mathcal{E}_r - c_1 a\tau_m)^2\right] \times \int_{v}^{v_{th}} \mathrm{d}v' H(v' - \mathcal{E}_r) \exp\left[\frac{1}{2\tau_m(2c_2D)}\left(v' - \mathcal{E}_r - c_1 a\tau_m\right)^2\right] \mathrm{d}v'. \tag{73}$$

Appendix D. Demonstration of instantaneous limit

In order to simplify notation we consider the case of excitatory input only. In the case of instantaneous synaptic kinetics, $V(t)$ obeys

$$\frac{\mathrm{d}V}{\mathrm{d}t} = -\frac{1}{\tau_m}\,(V - \mathcal{E}_r) + \sum_k A_k \delta(t - T_k), \tag{74}$$

where A_k and T_k are as defined in section 2.1.

The derivation of the excitatory flux term is analogous to that for the conductance driven synapse in Nykamp and Tranchina (2000). When an event arrives, V jumps by a random amount A_e. Thus, an excitatory flux across voltage v is contributed by neurons in a small neighbourhood ($\mathrm{d}v'$) around $v' < v$ whenever $A_e > v - v'$, which occurs with probability $\tilde{F}_{A_e}(v - v')$. Given that a synaptic event has occurred, the probability that a neuron in this particular neighbourhood will receive synaptic input is $\rho(v', t)\,\mathrm{d}v'$. The probability per unit time of an event is $\nu_e(t)$. Therefore, the excitatory flux $J_e(v, t)$ is given by

$$J_e(v, t) = \nu_e(t) \int_{-\infty}^{v} \tilde{F}_{A_e}(v - v')\rho(v', t)\,\mathrm{d}v' \tag{75}$$

$$= \nu_e(t) \int_{0}^{\infty} \tilde{F}_{A_e}(x)\rho(v - x, t)\,\mathrm{d}x. \tag{76}$$

In the non-instantaneous kinetics case, we have

$$J_e(v, t) = \int_{-\infty}^{t} \mathrm{d}t' \nu_e(t') h_e(t - t') \int_{0}^{\infty} \mathrm{d}x\, x f_{A_e}(x)\rho(v - x q_e(t - t')). \tag{77}$$

Expanding $\rho(v - x q_e(t - t'))$ in a Taylor series about v gives

$$J_e(v, t) = \int_{-\infty}^{t} \mathrm{d}t' \nu_e(t') \sum_{k=0}^{\infty} \frac{\partial^k \rho}{\partial v^k} h_e(t - t') q_e^k(t - t') \int_{0}^{\infty} \mathrm{d}x\, x^{k+1} f_{A_e}(x) \frac{(-1)^k}{k!}. \tag{78}$$

We show below that for $h_e(t)$ given by a sum of exponentials, in the limit of instantaneous synaptic kinetics, where $h_e(t) \to \delta(t)$, $h_e(t) q_e^k(t) \to \frac{1}{k+1}\delta(t)$. If we use this fact in (78), $J_e(v, t)$ in this limit becomes

$$J_e(v, t) = \nu_e(t) \sum_{k=0}^{\infty} \frac{\partial^k \rho}{\partial v^k} \int_{0}^{\infty} \mathrm{d}x \frac{x^{k+1}}{(k+1)!} (-1)^k f_{A_e}(x). \tag{79}$$

Integrating by parts yields

$$J_e(v, t) = \nu_e(t) \int_{0}^{\infty} \mathrm{d}x\, \tilde{F}_{A_e}(x) \sum_{k=0}^{\infty} \frac{\partial^k \rho}{\partial v^k} \frac{(-x)^k}{k!} \tag{80}$$

$$= \nu_e(t) \int_{0}^{\infty} \mathrm{d}x\, \tilde{F}_{A_e}(x)\rho(v - x, t) \tag{81}$$

which is the same as the flux for the instantaneous synapse case given in equation (76).

We show that $h_e(t)q_e^k(t) \to \frac{1}{k+1}\delta(t)$ in the limit of instantaneous synaptic kinetics, for any $h_e(t)$ that is a sum of exponentials

$$h_e(t) = \sum_k a_k \alpha_k \exp(-\alpha_k t) H(t), \tag{82}$$

where $\sum_k a_k = 1$, by virtue of the fact that $h_e(t)$ has unit integral, and $\mathcal{R}e(\alpha_k)$ is positive. In the instantaneous limit $\mathcal{R}e(\alpha_k) \to \infty$ for all k and $h_e(t) \to \delta(t)$. By definition, $q_e(t) = h_e(t) * (H(t)\exp(-\frac{t}{\tau_m}))$, which approaches $H(t)\exp(-\frac{t}{\tau_m})$ as $h_e(t)$ approaches $\delta(t)$. Since the decay of $h_e(t)$ becomes more rapid as the synaptic kinetics become faster, so must the product function $h_e(t)q_e^k(t)$. Thus, $h_e(t)q_e^k(t)$ must approach $z_k\delta(t)$, but the constant z_k is not obvious. The constant z_k is given by

$$z_k = \lim_{h_e(t)\to\delta(t)} \int_{-\infty}^{\infty} h_e(t) q_e^k(t)\, \mathrm{d}t. \tag{83}$$

Evaluation of the integral (83) is greatly simplified by using the fact that

$$\frac{\mathrm{d}q_e}{\mathrm{d}t} = -\frac{1}{\tau} q_e + h_e. \tag{84}$$

Thus,

$$h_e(t)q_e^k(t) = q_e^k(t)\frac{\mathrm{d}q_e}{\mathrm{d}t} + \frac{1}{\tau_m} q_e^{k+1} \tag{85}$$

$$= \frac{1}{k+1}\frac{\mathrm{d}q_e^{k+1}}{\mathrm{d}t} + \frac{1}{\tau_m} q_e^{k+1}. \tag{86}$$

Substituting this expression for $h_e(t)q_e^k(t)$ into (83) gives

$$\int_{-\infty}^{\infty} h_e(t) q_e^k(t)\, \mathrm{d}t = \frac{1}{k+1}\int_{-\infty}^{\infty} \frac{\mathrm{d}q_e^{k+1}}{\mathrm{d}t}\, \mathrm{d}t + \frac{1}{\tau_m}\int_{-\infty}^{\infty} q_e^{k+1}(t)\, \mathrm{d}t \tag{87}$$

$$= \frac{1}{\tau_m}\int_{-\infty}^{\infty} q_e^{k+1}(t)\, \mathrm{d}t. \tag{88}$$

Since $q_e(t)$ is a simple convolution of exponentials it can be easily found:

$$q_e(t) = \sum_k a_k \frac{\alpha_k \tau_m}{\alpha_k \tau_m - 1}\left(\exp\left(-\frac{t}{\tau_m}\right) - \exp(-\alpha_k t)\right). \tag{89}$$

For large $\mathcal{R}e(\alpha_k)$, ignoring terms $\mathrm{O}(\|\alpha_k\|^{-1})$, $q_e(t)$ can be approximated by

$$q_e(t) \approx \sum_k a_k \left(\exp\left(-\frac{t}{\tau_m}\right) - \exp(-\alpha_k t)\right) \tag{90}$$

$$= \exp\left(-\frac{t}{\tau_m}\right) - \sum_k a_k \exp(-\alpha_k t), \tag{91}$$

where we have used that $\sum_k a_k = 1$. When $q_e^{k+1}(t)$ is expanded out, it is clear from approximation (89) that, as $\mathcal{R}e(\alpha_k) \to \infty$, only the first term, $\exp(-\frac{t}{\tau_m})$, contributes to the integral (88), since all other terms decay instantaneously and have zero integral in the limit. Therefore,

$$z_k = \lim_{h_e(t)\to\delta(t)} \int_{-\infty}^{\infty} h_e(t) q_e^k(t)\, \mathrm{d}t \tag{92}$$

$$= \lim_{h_e(t)\to\delta(t)} \frac{1}{\tau_m}\int_{-\infty}^{\infty} q_e^{k+1}(t)\, \mathrm{d}t \tag{93}$$

$$= \frac{1}{\tau_m}\int_{-\infty}^{\infty} \exp\left(-(k+1)\frac{t}{\tau_m}\right) \mathrm{d}t \tag{94}$$

$$= \frac{1}{k+1}. \tag{95}$$

Appendix E. Moment matching technique

We now show how the coefficients in the evolution equation for $\rho_V(v,t)$ can be found by a moment matching technique. The SDE (1) describes the evolution of a neuron's membrane potential, $V(t)$. As such, it completely specifies the evolution of the moments of $V(t)$. The evolution equations for the mean $\mu_V(t)$ and variance $\sigma_V^2(t)$ of the membrane potential are derived in sections E.1.2 and E.1.3. The evolution equation for the third moment, $K_V^3(t)$, is calculated in a similar fashion. We state the result for $K_V^3(t)$ and omit the details.

Suppose one assumes that the evolution equation for $\rho_V(v,t)$ can be approximated by

$$\frac{\partial \rho_V}{\partial t} = -\frac{\partial}{\partial v}\left\{-\frac{1}{\tau_m}(v-\mathcal{E}_\mathrm{r})\rho_V(v,t)+\alpha(t)\rho_V(v,t)+\beta(t)\frac{\partial \rho_V}{\partial v}(v,t)+\gamma(t)\frac{\partial^2 \rho_V}{\partial v^2}(v,t)\right\}. \quad (96)$$

In the section E.1.1 we show that in order to find the mean of the membrane potential, we need to know $\alpha(t)$. We also show that, once the mean is known, $\beta(t)$ is required for finding the variance. In a similar manner, $\gamma(t)$ is needed in order to find the third moment, $K_V^3(t)$, of the membrane potential. However, the coefficients $\alpha(t),\ \beta(t),\ \gamma(t)$ are not known.

E.1. Derivation of evolution equations

In this section, we show the derivation of the evolution equations for the moments of the membrane potential from both the SDE (1) and the PDE (96). Given these evolution equations, we may then compare terms to solve for the coefficients of the PDE (96).

E.1.1. Moments from the PDE (96). To compute the evolution of the mean and variance, we make use of the reduced form of the conservation equation (20) $\frac{\partial \rho_V}{\partial t} = -\frac{\partial J_V}{\partial v}$, where $J_V(v,t)$ is given by equation (96):

$$\begin{aligned}
\frac{\mathrm{d}\mu_V}{\mathrm{d}t} &= \frac{\mathrm{d}}{\mathrm{d}t}\mathbb{E}(V) && (97)\\
&= \int v\frac{\partial \rho_V}{\partial t}\,\mathrm{d}v && (98)\\
&= \int -v\frac{\partial J_V}{\partial t}\,\mathrm{d}v && (99)\\
&= \int vJ_V\,\mathrm{d}v && (100)\\
&= \int v\left(-\frac{1}{\tau_m}(v-\mathcal{E}_\mathrm{r})\rho_V+\alpha(t)\rho_V+\beta(t)\frac{\partial \rho_V}{\partial v}+\gamma(t)\frac{\partial^2 \rho_V}{\partial v^2}\right)\mathrm{d}v && (101)\\
&= -\frac{1}{\tau_m}(\mu_V-\mathcal{E}_\mathrm{r})+\alpha(t). && (102)
\end{aligned}$$

Similarly, we can find an evolution equations for the variance;

$$\begin{aligned}
\frac{\mathrm{d}\sigma_V^2}{\mathrm{d}t} &= \frac{\mathrm{d}}{\mathrm{d}t}\mathbb{E}((V-\mu_V)^2) && (103)\\
&= \frac{\mathrm{d}}{\mathrm{d}t}\mathbb{E}[V^2]-2\mu_V(t)\frac{\mathrm{d}\mu_V}{\mathrm{d}t}. && (104)
\end{aligned}$$

The computation of the expected value of V^2 follows the same methodology as that for the expected value of $V(t)$. Then, $\frac{\mathrm{d}\mu_V}{\mathrm{d}t}$ is replaced with the previously found expression to achieve

$$\frac{\mathrm{d}\sigma_V^2}{\mathrm{d}t} = -\frac{2}{\tau_m}\sigma_V^2-2\beta(t). \quad (105)$$

E.1.2. The evolution of the mean membrane potential. We derive an evolution equation for the mean membrane potential by finding the expected value of the membrane potential from the SDE (1). By conditioning on the number of event arrivals in (108), we can use that $A^k_{\mathrm{e/i}}$, $T^k_{\mathrm{e/i}}$ are independent identically distributed random variables in (109):

$$\frac{\mathrm{d}\mu_V(t)}{\mathrm{d}t} = \mathbb{E}\left[\frac{\mathrm{d}V}{\mathrm{d}t}\right] \tag{106}$$

$$= -\frac{1}{\tau_m}(\mu_V - \mathcal{E}_{\mathrm{r}}) + \mathbb{E}\left[\sum_{k=1}^{N} A^k h(t - T^k)\right] \tag{107}$$

$$= -\frac{1}{\tau_m}(\mu_V - \mathcal{E}_{\mathrm{r}}) + \mathbb{E}\left[\mathbb{E}\left[\sum_{k=1}^{n} A^k h(t - T^k)\middle| N = n\right]\right] \tag{108}$$

$$= -\frac{1}{\tau_m}(\mu_V - \mathcal{E}_{\mathrm{r}}) + \mathbb{E}\left[n \iint a\, h(t - t')\frac{\nu(t')}{\int \nu(s)\,\mathrm{d}s} f_A(a)\,\mathrm{d}a\,\mathrm{d}t'\right] \tag{109}$$

$$= -\frac{1}{\tau_m}(\mu_V - \mathcal{E}_{\mathrm{r}}) + \mu_A \int h(t - t')\nu(t')\,\mathrm{d}t' \tag{110}$$

$$= -\frac{1}{\tau_m}(\mu_V - \mathcal{E}_{\mathrm{r}}) + \mu_A\Big(h * \nu\Big)(t). \tag{111}$$

E.1.3. The evolution of the variance of the membrane potential. Using the analytic solution for the SDE (1),

$$V(t) = \mathcal{E}_{\mathrm{r}} + \frac{1}{\tau_m}\mathrm{e}^{-\frac{t}{\tau_m}} * I(t), \tag{112}$$

we derive an evolution equation for the variance of the membrane potential in a similar manner as in the previous section:

$$\frac{\mathrm{d}\sigma_V^2(t)}{\mathrm{d}t} = \mathbb{E}\left[\frac{\mathrm{d}}{\mathrm{d}t}\Big(V^2 - \mu_V^2\Big)\right] \tag{113}$$

$$= \mathbb{E}\left[2V\frac{\mathrm{d}V}{\mathrm{d}t} - 2\mu_V\frac{\mathrm{d}\mu_V}{\mathrm{d}t}\Big)\right] \tag{114}$$

$$= -\frac{2}{\tau_m}(\mu_{V^2} - \mathcal{E}_{\mathrm{r}}\mu_V) + 2\mathbb{E}\left[V(t)\sum_{k=1}^{N} A^k h(t - T^k)\right] - \left(-\frac{2}{\tau_m}(\mu_V^2 - \mathcal{E}_{\mathrm{r}}\mu_V) + 2\mu_V\mu_A(h * \nu)(t)\right) \tag{115}$$

$$= -\frac{2}{\tau_m}\sigma_V^2 + 2\mu_{A^2}(qh * \nu). \tag{116}$$

By comparing the evolution equations for the moments found from the SDE (10) and PDE (96) we find these coefficients:

$$\alpha(t) = \int_{-\infty}^{t} h_e(t - t')\nu_e(t')\,\mathrm{d}t' \tag{117}$$

$$\beta(t) = \int_{-\infty}^{t} q_e(t - t')h_e(t - t')\nu_e(t')\,\mathrm{d}t' \tag{118}$$

$$\gamma(t) = \int_{-\infty}^{t} q_e^2(t - t')h_e(t - t')\nu_e(t')\,\mathrm{d}t'. \tag{119}$$

These coefficients are the same as those in (45).

Appendix F. First-order kinetics example

Throughout this paper, we have used first-order kinetics as a specific example and for all simulations. For first-order kinetics, the unitary synaptic current event is described by a single exponential as in equation (8):

$$h_{\mathrm{e/i}}(t) = \frac{1}{\tau_{\mathrm{d}}^{\mathrm{e/i}}} \mathrm{e}^{-\frac{t}{\tau_{\mathrm{d}}^{\mathrm{e/i}}}} H(t). \tag{120}$$

In this appendix we show, using these kinetics, how to find $\mu_{A_{\mathrm{e/i}}}$ and then discuss some practical issues for implementing these kinetics efficiently.

From the original SDE (1), we can find the time it takes for the neuron to reach its peak response to an unitary event. That is, if an event arrives at time T, for what value Δt_{peak} is $\Delta V = |V(T + \Delta t_{\mathrm{peak}}) - V(T)|$ maximal? For these kinetics, the time is found to be

$$\Delta t_{\mathrm{peak}}^{\mathrm{e}} = \frac{\tau_{\mathrm{d}}^{\mathrm{e}} \tau_m}{\tau_m - \tau_{\mathrm{d}}^{\mathrm{e}}} \ln\left(\frac{\tau_m}{\tau_{\mathrm{d}}^{\mathrm{e}}}\right) \geqslant 0. \tag{121}$$

If we specify a mean peak voltage change, $\Delta v_{\mathrm{peak}}^{\mathrm{e}}$, then we can evaluate the unitary event response of (1) at Δt_{peak} to solve for $\mu_{A_{\mathrm{e}}}$:

$$\mu_{A_{\mathrm{e}}} = \frac{\Delta v_{\mathrm{peak}}^{\mathrm{e}} \left(\frac{\tau_{\mathrm{d}}^{\mathrm{e}} - \tau_m}{\tau_m}\right)}{\left(\frac{\tau_{\mathrm{d}}^{\mathrm{e}}}{\tau_m}\right)^{\frac{\tau_m}{\tau_m - \tau_{\mathrm{d}}^{\mathrm{e}}}} - \left(\frac{\tau_{\mathrm{d}}^{\mathrm{e}}}{\tau_m}\right)^{\frac{\tau_{\mathrm{d}}^{\mathrm{e}}}{\tau_m - \tau_{\mathrm{d}}^{\mathrm{e}}}}}. \tag{122}$$

The solution to the SDE (1) is

$$V(t) = \mathcal{E}_{\mathrm{r}} + \sum_{k=1}^{N_{\mathrm{e}}} A_{\mathrm{e}}^k q_{\mathrm{e}}(t - T_{\mathrm{e}}^k) - \sum_{k=1}^{N_{\mathrm{i}}} A_{\mathrm{e}}^k q_{\mathrm{i}}(t - T_{\mathrm{i}}^k) \tag{123}$$

where

$$q(t) = h(t) * \mathrm{e}^{-\frac{t}{\tau_m}} \tag{124}$$

$$q(t) = \frac{\tau_m}{\tau_m - \tau_{\mathrm{d}}^{\mathrm{e}}} \left(\mathrm{e}^{-\frac{t}{\tau_m}} - \mathrm{e}^{-\frac{t}{\tau_{\mathrm{d}}^{\mathrm{e}}}}\right) \tag{125}$$

$$= \frac{1}{1 - \frac{\tau_{\mathrm{d}}^{\mathrm{e}}}{\tau_m}} \mathrm{e}^{-\frac{t}{\tau_{\mathrm{d}}^{\mathrm{e}}}} \left(\mathrm{e}^{-t\left(\frac{1}{\tau_m} - \frac{1}{\tau_{\mathrm{d}}^{\mathrm{e}}}\right)} - 1\right), \tag{126}$$

and $*$ denotes the convolution operator.

In order to evolve the coefficients of advection, diffusion and dispersion, we need to know

$$q^k(t) = \left(\frac{1}{1 - \frac{\tau_{\mathrm{d}}^{\mathrm{e}}}{\tau_m}}\right)^k \mathrm{e}^{-k\frac{t}{\tau_{\mathrm{d}}^{\mathrm{e}}}} \left(\sum_{j=0}^{k} \binom{k}{j} (-1)^{k-j} \mathrm{e}^{-jt\left(\frac{1}{\tau_m} - \frac{1}{\tau_{\mathrm{d}}^{\mathrm{e}}}\right)}\right) \tag{127}$$

$$q^k(t)h(t) = \frac{1}{\tau_{\mathrm{d}}^{\mathrm{e}}} \left(\frac{1}{1 - \frac{\tau_{\mathrm{d}}^{\mathrm{e}}}{\tau_m}}\right)^k \mathrm{e}^{-(k+1)\frac{t}{\tau_{\mathrm{d}}^{\mathrm{e}}}} \left(\sum_{j=0}^{k} \binom{k}{j} (-1)^{k-j} \mathrm{e}^{-jt\left(\frac{1}{\tau_m} - \frac{1}{\tau_{\mathrm{d}}^{\mathrm{e}}}\right)}\right). \tag{128}$$

Since the waveform $h_{\mathrm{e}}(t)$ is given by an exponential, the convolutions expressed in equation (45) are convolutions of exponentials with $v_{\mathrm{e}}(t)$. Thus, these convolutions can be written as ODEs which are much more numerically efficient to implement than convolution integrals:

$$\frac{\mathrm{d}a}{\mathrm{d}t} = -\frac{1}{\tau_s} a + \frac{\mu_A}{\tau_s} v(t) \tag{129}$$

$$D(t) = -\frac{\mu_{A^2}}{\tau_s}\frac{\tau_m}{\tau_m - \tau_s}(D_1(t) - D_2(t)) \tag{130}$$

$$\frac{\mathrm{d}D_1}{\mathrm{d}t} = -\left(\frac{1}{\tau_m} + \frac{1}{\tau_s}\right) D_1(t) + \nu(t) \tag{131}$$

$$\frac{\mathrm{d}D_2}{\mathrm{d}t} = -\frac{2}{\tau_s} D_2(t) + \nu(t) \tag{132}$$

$$F(t) = \frac{1}{2}\frac{\mu_{A^3}}{\tau_s}\frac{\tau_m^2}{(\tau_m - \tau_s)^2}\Big(F_1(t) + F_2(t) - 2F_3(t)\Big) \tag{133}$$

$$\frac{\mathrm{d}F_1}{\mathrm{d}t} = -\frac{3}{\tau_s} F_1(t) + \nu(t) \tag{134}$$

$$\frac{\mathrm{d}F_2}{\mathrm{d}t} = -\left(\frac{2}{\tau_m} + \frac{1}{\tau_s}\right) F_2(t) + \nu(t) \tag{135}$$

$$\frac{\mathrm{d}F_3}{\mathrm{d}t} = -\left(\frac{1}{\tau_m} + \frac{2}{\tau_s}\right) F_3(t) + \nu(t). \tag{136}$$

References

Abbott L F and van Vreeswijk C 1993 Asynchronous states in networks of pulse-coupled oscillators *Phys. Rev.* E **48** 1483–90

Adorján P, Barna G, Érdi P and Obermayer K 1999 A statistical neural field approach to orientation selectivity *Neurocomputing* at press

Barna G, Gröbler T and Érdi P 1998 Statistical model of the hippocampal ca3 region, ii. the population framework: model of rhythmic activity in ca3 slice *Biol. Cybern.* **79** 309–21

Bressloff P C and Coombes S 2000 Dynamics of strongly coupled spinking neurons *Neural Comput.* **12** 91–129

Brunel N and Hakim V 1999 Fast global oscillations in networks of integrate-and-fire neurons with low firing rates *Neural Computation* **11** 1621–71

Chawanya T, Aoyagi A, Nishikawa I, Okuda K and Kuramoto Y 1993 A model for feature linking via collective oscillations in the primary visual cortex *Biol. Cybern.* **68** 483–90

Fain G L 1999 *Molecular and Cellular Physiology of Neurons* (Cambridge, MA: Harvard University Press)

Gerstner W 1995 Time structure of the activity in neural network models *Phys. Rev.* E **51** 738–58

——1999 Population dynamics of spiking neurons: fast transients, asynchronous states, and locking *Neural Comput.* **12** 43–90

Gerstner W and van Hemmen J 1994 Coding and information processing in neural networks *Models of Neural Networks* vol 2, ed E Domany, J van Hemmen and K Schulten (New York: Springer) pp 1–93

Grzywacz N M, Hillman P and Knight B W 1988 The quantal source of area supralinearity of flash responses in Limulus photoreceptors *J. Gen. Physiol.* **91** 659–84

Hansel D, Mato G, Meunier C and Neltner L 1998 On numerical simulations of integrate-and-fire neural networks *Neural Comput.* **10** 467–83

Knight B, Omurtag A and Sirovich L 2000 The approach of a neuron population firing rate to a new equilibrium: an exact theoretical result *Neural Comput.* **12** 1045–55

Knight B W 1972a Dynamics of encoding in a population of neurons *J. Gen. Physiol.* **59** 734–66

——1972b The relationship between the firing rate of a single neuron and the level of activity in a population of neurons. experimental evidence for resonant enhancement in the population response *J. Gen. Physiol.* **59** 767–78

——2000 Dynamics of encoding in neuron populations: some general mathematical features *Neural Comput.* **12** 473–518

Knight B W, Manin D and Sirovich L 1996 Dynamical models of interacting neuron populations *Symposium on Robotics and Cybernetics: Computational Engineering in Systems Applications* ed E C Gerf (France: Cite Scientifique)

Koch C 1999 *Biophysics of Computation: Information Processing in Single Neurons* (New York: Oxford University Press)

Kuramoto Y 1991 Collective synchronization of pulse-coupled oscillators and excitable units *Physica* D **50** 15–30

Nykamp D Q and Tranchina D 2000 A population density approach that facilitates large-scale modelling of neural networks: Analysis and an application to orientation tuning *J. Comput. Neurosci.* **8** 19–50

Nykamp D Q and Tranchina D 2001 A population density approach that facilitates large-scale modelling of neural networks: extension to slow inhibitory synapses *Neural Comput.* **13** 511–46

Omurtag A, Knight B W and Sirovich L 2000 On the simulation of large populations of neurons *J. Comput. Neurosci.* **8** 51–63

Pham J, Pakdaman K, Champagnat J and Vibert J 1998 Activity in sparsely connected excitatory neural networks: effect of connectivity *Neural Networks* **11** 415–34

Sirovich L, Knight B and Omurtag A 2000 Dynamics of neuronal populations: the equilibrium solution *SIAM* at press

Somers D C, Nelson S B and Sur M 1995 An emergent model of orientation selectivity in cat visual cortical simple cells *J. Neurosci.* **15** 5448–65

Strogatz S H and Mirollo R E 1991 Stability of incoherence in a population of coupled oscillators *J. Stat. Phys.* **63** 613–35

Treves A 1993 Mean-field analysis of neuronal spike dynamics *Network* **4** 259–84

Tuckwell H C 1988 *Introduction to Theoretic Neurobiology* vol 2 (New York: Cambridge University Press) pp 111–89

Wang X J 1999 Synaptic basis of cortical persistent activity: the importance of NMDA receptors to working memory *J. Neurosci.* **19** 9587–603

Wilbur W and Rinzel J 1982 An analysis of stein's model for stochastic neural excitation *Biol. Cyber.* **45** 107–14

——1983 A theoretical basis for large coefficient of variation and bimodality in neuronal interspike interval distributions *J. Theor. Biol.* **105** 345–68